LAWRENCE
LIVERMORE
NATIONAL
LABORATORY

LLNL-JRNL-872921

Recent Warming of Southern Hemisphere Subtropical Lower Stratosphere and Antarctic Ozone Healing

A. Sweeney, Q. Fu, S. Solomon, S. Po-Chedley, W. Randel, A. Steiner, J. M. Wallace, P. Lin, T. Birner, S. Davis, P. Wang

March 12, 2025

AGU Advances

Disclaimer

Recent Warming of the Southern Hemisphere Subtropical Lower Stratosphere and Antarctic Ozone Healing

Aodhan Sweeney[1], Qiang Fu[1], Susan Solomon[2], Stephen Po-Chedley[3], William J. Randel[4], Andrea Steiner[5], Pu Lin[6], Thomas Birner[7,8], Sean Davis[9], Peidong Wang[2]

[1]Department of Atmospheric and Climate Science, University of Washington, Seattle, WA 98195

[2] Department of Earth, Atmospheric, and Planetary Sciences, Massachusetts Institute of Technology, Cambridge, MA 02139

[3]Program for Climate Model Diagnosis and Intercomparison, Lawrence Livermore National Laboratory, Livermore, CA, USA

[4]NSF National Center for Atmospheric Research, Boulder, CO 80307

[5]Wegener Center for Climate and Global Change, University of Graz, Graz, Austria

[6]Program in Atmospheric and Oceanic Sciences, Princeton University, Princeton, NJ, USA

[7]Meteorological Institute, Ludwig-Maximilians-Universität München, Munich, Germany

[8]Institute of Atmospheric Physics, Deutsches Zentrum für Luft- und Raumfahrt, Oberpfaffenhofen, Germany

[9]NOAA Chemical Sciences Laboratory, Boulder, CO 80305

Corresponding authors: Aodhan Sweeney (aodhan@uw.edu) and Qiang Fu (qfu@uw.edu)

Key Points:

- The warming of the Southern Hemisphere (SH) subtropical lower stratosphere over 2002-2022 is linked to Brewer-Dobson Circulation slowdown
- These circulation changes also cool the Antarctic lower stratosphere and mask the Antarctic ozone healing from October to December
- Removing circulation changes eliminates SH subtropical stratospheric warming and reveals Antarctic warming and enhanced ozone healing

Abstract

Observed temperature changes from 2002-2022 reveal a pronounced warming of the Southern Hemisphere (SH) subtropical lower stratosphere, and a cooling of the Antarctic lower stratosphere. In contrast, model simulations of 21st-century stratospheric temperature changes show widespread cooling driven by increasing greenhouse gases, with local warming in the Antarctic lower stratosphere due to ozone healing. We provide evidence that these discrepancies between observed and simulated stratospheric temperature changes are linked to a slowdown of the Brewer-Dobson Circulation (BDC), particularly in the SH. These changes in the stratospheric circulation are strongest from October through December. This altered circulation warms the SH subtropical lower stratosphere while cooling the Antarctic lower stratosphere, canceling and even

reversing the Antarctic ozone recovery that would have occurred in its absence during this period. When circulation changes are accounted for, the SH subtropical lower-stratospheric warming is removed, and Antarctic lower-stratospheric warming is revealed with enhanced ozone healing, highlighting the crucial role of the stratospheric circulation in shaping temperature and ozone changes.

Plain Language Summary

Climate models predict that rising greenhouse gas levels cool the stratosphere, while the healing of the Antarctic ozone hole—driven by the reduction of ozone-depleting substances under the Montreal Protocol since the beginning of the 21st century—should warm the Antarctic lower stratosphere. However, observations for the period from 2002 to 2022 reveal unexpected changes: warming in the Southern Hemisphere (SH) subtropical lower stratosphere and cooling over Antarctica. This study identifies the cause as a slowdown in stratospheric circulation that moves stratospheric air and chemicals from low to high latitudes. These circulation changes, most pronounced from October to December, lead to warming in the subtropical lower stratosphere of the Southern Hemisphere and cooling in the Antarctic lower stratosphere. They also mask the anticipated ozone recovery over Antarctica during this period. Accounting for these circulation changes removes the anomalous warming of the SH subtropical lower stratosphere and reveals an obvious Antarctic lower stratospheric warming and enhanced ozone recovery. These findings highlight the crucial role of the stratospheric circulation in shaping temperature and ozone changes.

1 Introduction

Observations largely confirm the expected response to increased greenhouse gas concentrations (GHGs) of tropospheric warming and stratospheric cooling (e.g., Manabe and Weatherald, 1967; Karoly et al., 1994; Fu et al., 2004; Vallis et al., 2015; Khaykin et al., 2017; Steiner et al., 2020b; Ladstädter et al., 2023; Santer et al., 2023). However, from 2002-2022, an unexpected anomalous warming of the Southern Hemisphere (SH) subtropical lower stratosphere was found in Radio Occultation (RO) observations (see Fig. 1A) (Shangguan et al., 2019; Gleisner et al., 2022; Ladstädter et al., 2023; IPCC, 2023). The underlying cause of this Anomalous Warming of the Lower Stratosphere (abbreviated as AWLS) remains unknown.

Over the same period, the observed Antarctic lower stratosphere cooled in contrast to the expected warming induced by ozone recovery (Hu et al., 2011; Maycock, 2016; Solomon et al., 2017; Randel et al., 2017; Maycock et al., 2018; Fu et al., 2019; Ladstädter et al., 2023). Observed warming in the AWLS region and cooling in the Antarctic lower stratosphere vary seasonally, but the largest changes in both regions occur from October-December (Ladstädter et al., 2023). This observed dipolar change in lower stratospheric temperature between the subtropical SH and Antarctic might be evidence for changes in the SH Brewer-Dobson Circulation (BDC) which can link variability between the low and high latitude stratosphere (Butchart, et al., 2014).

The BDC plays a crucial role in regulating the distribution and transport of ozone, which is produced at lower latitudes and moved poleward by the circulation (Brewer 1949; Dobson, 1956; Perliski et al., 1989). The SH-BDC can also change the temperature of the Antarctic stratospheric vortex, which determines the efficiency of chemical ozone depletion (Solomon et al., 1986; WMO, 2022). While Antarctic ozone healing since 2000 has been detected during September in line with model simulations, recovery from October to December is not observed (e.g., see Fig. 4-16 in WMO, 2022) (Solomon et al., 2016; Solomon et al., 2017; Wang et al., 2025; WMO, 2022; Chipperfield et al., 2017; Kuttippurath and Nair, 2017; Stone et al., 2021; Kessenich et al., 2023; Chipperfield and Bekki, 2024). Dynamical activity during these months strongly impacts temperature and ozone changes (e.g., Randel and Wu 2015; Dhomse et al., 2018; Robertson et al., 2023). In addition, enhanced aerosol loadings and chemical processes related to wildfires and volcanoes may also contribute to the discrepancies (e.g., Stone et al., 2021; Bernath et al., 2022; Yook et al., 2022; Solomon et al., 2022; Solomon et al., 2023; Stocker et al., 2021; Wang et al., 2023; Zhang et al., 2024; Stocker et al., 2024). Recently, Wang et al. (2025) demonstrated a striking agreement in the observed and simulated fingerprint pattern of Antarctic ozone response to decreasing ozone depleting substances (ODSs) since 2005, offering strong evidence that Antarctic ozone recovery is underway. They also discovered that ODS forcing has amplified the Antarctic ozone internal variability during austral spring compared to the pre-ODS era, affecting the detection of ozone recovery.

Here we show that the AWLS is linked to a slowdown of the BDC, particularly in the SH. We focus mainly on 2002-2022 but also consider other time periods. These circulation changes not only warm the AWLS region but also cool the Antarctic lower stratosphere. We also explore the implications of this SH-BDC slowdown for ozone and indicate that it can obscure signs of Antarctic ozone healing from October to December, depending on the time period

considered. While external forcing associated with GHGs and ODSs remains relatively stable regardless of the chosen time periods, internal variability is highly sensitive to start and end dates as well as the duration of the period. By accounting for this decadal variation in the BDC, we bring observed and simulated temperature and ozone changes for 2002-2022 into an overall agreement.

Section 2 describes the data and methods used. In Section 3, we first partition temperature changes from 2002-2022 into those related to the AWLS and those that are not. We then investigate the seasonal variation of temperature and ozone changes, as well as the influence of the stratospheric circulation on these changes, followed by a comparison with simulated changes from a representative climate model. The discussion & sensitivity analysis in Section 4 establishes context for our findings. Finally, Section 5 summarizes our results and highlights their importance.

2 Data and Methods

We analyze interannual variability and decadal trends of stratospheric variables using monthly anomalies, calculated by removing the 2002-2022 monthly climatology from the monthly mean data. We removed interannual variability associated with the El Niño Southern Oscillation (ENSO) and the Quasi-Biennial Oscillation (QBO) using a multiple linear regression (MLR), which was fitted to the anomalies of stratospheric variables and then subtracted (Randel and Wu, 2015; Tseng and Fu, 2017; Steiner et al., 2020). ENSO is represented by the MEI-V2 index with a three-month lead to maximize its impact on the lower stratosphere (Wolter and Timlin, 2011; Ladstadter et al., 2023), and QBO is represented by the first two principal components of Singapore wind observations (Wallace et al., 1993). All results presented in this study have these modes of variability removed.

2.1 Observation and Reanalysis Datasets

This analysis uses observations of atmospheric temperature and trace gas species. Observations of temperature come from Radio Occultation (RO) measurements stored by the COSMIC Data Analysis and Archive Center (CDAAC) from 2002-2022. RO temperature measurements provide stable and accurate temperature observations of the upper-troposphere and lower-stratosphere (UTLS) region with high vertical resolution, allowing for detailed investigation of changes in this region (Kuo et al., 2004; Kursinski et al., 1997; Steiner et al., 2013; Khaykin et al., 2017; Leroy et al., 2018; Steiner et al., 2020a; Scherllin-Pirscher et al., 2021). Data was preprocessed using the level 2 DryPrf from all RO satellites. RO temperature profiles were binned into monthly-mean, zonal-mean temperature fields with 200 m vertical resolution and 7.5° latitudinal resolution.

Observations of stratospheric ozone and water vapor come from SWOOSH, a merged record derived from limb soundings and solar occultations spanning 1984 to present (Davis et al., 2016). We use SWOOSH V2.7 data from 2002-2022, which relies heavily on measurements from the Microwave Limb Sounder onboard the Aura satellite, launched in 2004 (Read et al., 2007; Livesey et al., 2021). The primary SWOOSH product used here is the monthly-mean, zonal-mean ozone and water vapor mixing ratios provided on pressure levels. Observed changes

in GHGs and chlorofluorocarbons (CFCs) come from the NOAA/ESRL Global Monitoring Laboratory archive based on the Mauna Loa station.

We also use the ERA5 reanalysis data for monthly-mean zonal wind and residual stream functions (replaced by ERA5.1 when available) (Hersbach et al., 2020). Temperature and zonal wind are the monthly average of 6-hourly data at a given latitude and pressure level. The residual stream function is calculated following Diallo et al. (2021) using the 6-hourly data. We also use the monthly mean sea level pressure (SLP) data from ERA5 to calculate the Southern Annular Mode (SAM) index using the first principal component of the 20°S-90°S SLP anomalies.

2.2 CESM1 WACCM Simulations

Simulations of the 10-member Community Earth System Model 1 (CESM1) Whole Atmosphere Community Climate Model 4 (WACCM) ensemble are analyzed. These simulations are documented in Zambri et al. (2021) and have GHG concentrations following historical and representative concentration pathway 6.0, and ODS concentrations are prescribed following the WMO (2011) (Meinshausen et al., 2011). These simulations have the same prescribed 28-month Quasi-Biennial Oscillation (QBO) and no prescribed solar cycle. Since these simulations have different ENSO and QBO cycles from observations, we create indices to represent these modes in each ensemble. For ENSO, we use the deviation from the ensemble mean of 500 hPa temperature from 15°S-15°N. For the QBO, we use the ensemble mean zonal wind at 10 and 30 hPa. These three predictors are then fit to each of the ensemble members and removed using a multiple linear regression.

2.3 NASA Langley Fu-Liou Radiation Model

We estimate temperature changes due to observed changes in GHGs (CO_2, CH_4, N_2O), CFCs, and stratospheric ozone and water vapor through radiative processes by using the NASA Langley Fu-Liou radiation model (Fu and Liou, 1992). Radiatively induced temperature changes are derived using the "Seasonally Evolving Fixed Dynamical Heating" approach, which fixes the dynamical heating so that the resulting temperature changes are the result of radiative processes (Forster and Shine, 1997; Fu et al., 2015; Ming and Hitchcock, 2022). Observed changes in GHGs, CFCs, and stratospheric O_3 and H_2O come from the datasets described in Section 2.1. Changes in well-mixed GHG concentrations are considered throughout the atmosphere, whereas changes in O_3 and H_2O are applied at and above the tropopause. Below the tropopause, water vapor, ozone, and temperature are held to their ERA5 climatological values.

2.4 Trend Calculations

The change for a given variable over a specific time period is quantified using the linear trend derived by applying ordinary least squares regression to the monthly anomalies. Uncertainty estimates for this regression are obtained accounting for the effective degrees of freedom after considering the lag-1 autocorrelation. Significance is defined at the 95% confidence level. Within any given period, the derived linear trend from observations reflects contributions from both external forcing and internal variability.

200 2.5 Circulation Regression
201
202 We aim to partition stratospheric variability into components that covary with
203 temperature in the AWLS region and those that do not. The zonal-mean monthly temperature
204 anomaly timeseries in the AWLS region, referred to as the "AWLS timeseries", serves as the
205 basis for this partitioning. This method can be applied to any variable of interest, such as
206 temperature, ozone, or zonal wind, using monthly anomalies from all months or from each
207 month individually. To carry out this partitioning, we start with zonal-mean monthly anomalies
208 after removing the QBO and ENSO, which we generically refer to as the "anomalies", and
209 proceed as follows:
210
211 1.) Detrend the anomalies at all latitudes (indexed by i) and heights (indexed by j), as
212 well as the AWLS timeseries.
213 2.) Regress the detrended anomalies at each location onto the detrended AWLS
214 timeseries to obtain the regression coefficients, m_{ij}.
215 3.) Multiply m_{ij} by the original (not detrended) AWLS timeseries to obtain the
216 component associated with "circulation variability". This is referred to as "circulation
217 variability" because m_{ij} is derived from detrended interannual timescales, where
218 stratospheric circulation is the dominant source of variability. Furthermore, as
219 demonstrated later, the trend in the AWLS timeseries is primarily driven by changes
220 in stratospheric circulation.
221 4.) Subtract the circulation variability from the original anomalies to obtain the
222 component that is independent of the AWLS timeseries.
223
224 We refer to this technique as the "circulation regression". Here, we assume that the
225 detrended AWLS timeseries serves as a good proxy for the interannual variability of
226 stratospheric circulation and we provide supporting evidence for this assumption in Section 3.
227
228 **3 Results**
229
230 Figure 1A shows the linear trends in zonal mean temperature between 8-30 km from the
231 RO record (Steiner et al., 2020b). The RO data document a statistically significant warming
232 below the tropopause with tropical tropospheric warming increasing with altitude between 8 and
233 13 km (Fu et al., 2004; Santer et al., 2005). Most of the stratosphere is cooling, while the AWLS
234 region (highlighted by red box in Fig. 1A) shows a strong warming above the SH subtropical
235 tropopause (Khaykin et al., 2017; Steiner et al., 2020b; Gleisner et al., 2022; Ladstädter, et al.,
236 2023; IPCC, 2021). The AWLS region is defined here as the region between 16.6 and 18.6 km
237 and 33.75°S to 11.25°S. Very similar changes are evident in the MSU/AMSU TLS
238 measurements at the same latitudes, suggesting that this warming is not an artifact of RO data
239 (see Fig. S1). Tropopause heights in this region show changes that are not statistically
240 significant, thus the AWLS is unlikely to be a direct manifestation of tropopause height changes
241 (Gao et al., 2015; Weyland et al., 2025). Fig. 1B shows the monthly temperature anomaly
242 timeseries in the AWLS region, revealing a warming of 0.4 K/decade since 2002 with the 95%
243 confidence interval of ±0.33 K/decade.
244

The observed RO temperature changes in Fig. 1A also show cooling in the Antarctic. Randel et al. (2017) reported Antarctic warming during 1998-2014 based on both MSU4 observations and WACCM simulations. The contrasting lower-stratospheric temperature trends over Antarctica between the RO observations (Fig. 1A) and the WACCM simulations (Fig. 9) for 2002-2022 may be attributed to internal variability. Notably, the blue dots in Fig. 1B highlight the concurrence of strong negative anomalies in the AWLS region with Antarctic Sudden Stratospheric Warmings (SSWs) in 2002 and 2019 (Newman and Nash, 2005; Xia et al., 2020; Lim et al., 2021). The apparent strong influence of Antarctic SSWs on this subtropical lower stratosphere suggests a close coupling of these regions through the SH-BDC (Zuev et al., 2024). This coupling is exemplified by the correlations between the AWLS region and the Antarctic lower stratosphere shown in Fig. 2.

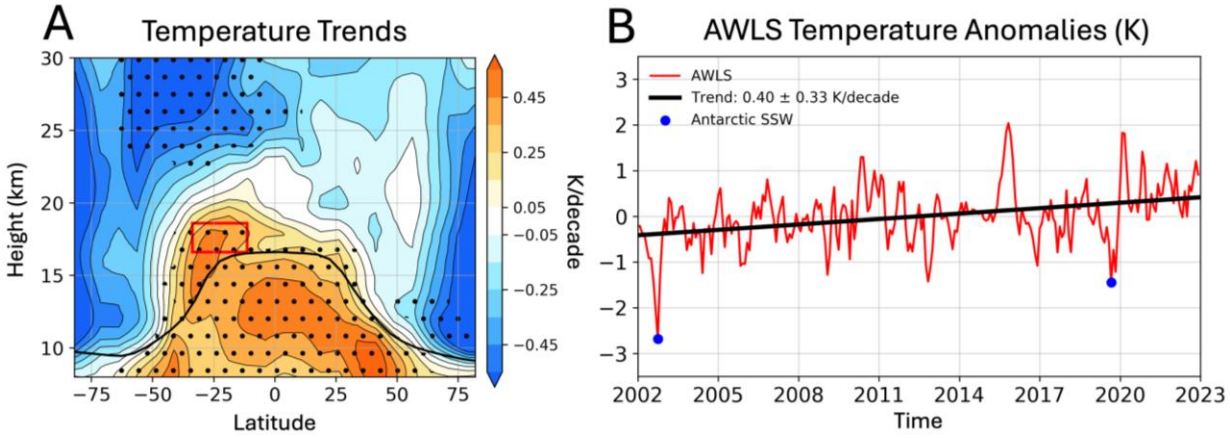

Figure 1: (A) Zonal-mean temperature trends from 8-30 km during 2002-2022 derived from RO data using anomalies from all months. Stippling indicates statistically significant trends at 95% confidence. The climatological lapse-rate tropopause height is indicated by the thick black line. The red box highlights the region with the Anomalous Warming of the Lower Stratosphere (AWLS). (B) monthly temperature anomaly timeseries in the AWLS region (i.e., the red box of panel A).

3.1 Partitioning Temperature Changes Based on Covariability with the AWLS

Figure 2A shows the correlation of detrended monthly temperature anomalies from 8-30 km with those of the AWLS region. Temperature anomalies in the AWLS region are strongly anticorrelated with those of the Antarctic lower stratosphere. This temperature covariability between the tropical and extratropical lower stratosphere is driven by variability in the BDC (Yulaeva et al., 1994). Fig. 2B shows the correlations with detrended temperature anomalies in an Antarctic lower stratospheric region (red box in Fig. 2B: 63.75°S-90°S and 13-17 km). In Fig. 2B, the region of the strongest anticorrelation with the Antarctic lower stratosphere is the AWLS region, highlighting the coupling of these two regions by the SH-BDC. Here, we emphasize that while the AWLS region was selected for its significant decadal trend (Fig. 1), its true importance lies not only in this pronounced trend but, more importantly, in its strong dynamic coupling with the Antarctic lower stratosphere (Fig. 2).

The AWLS region exhibits a weaker but significant anticorrelation with the Arctic (Fig. 2A), due to the teleconnection between the polar lower stratosphere and the subtropical lower

stratosphere in the opposite hemisphere (Fig. 2B). Figure S2 shows an analogous set of correlation maps with the Northern Hemisphere (NH) subtropics and Arctic, revealing similar connections. While this study focuses on the SH and associated stratospheric circulation changes, variations in the NH BDC are an integral part of the overall picture, as discussed in Sections 3.2, 4.2, and 4.5.

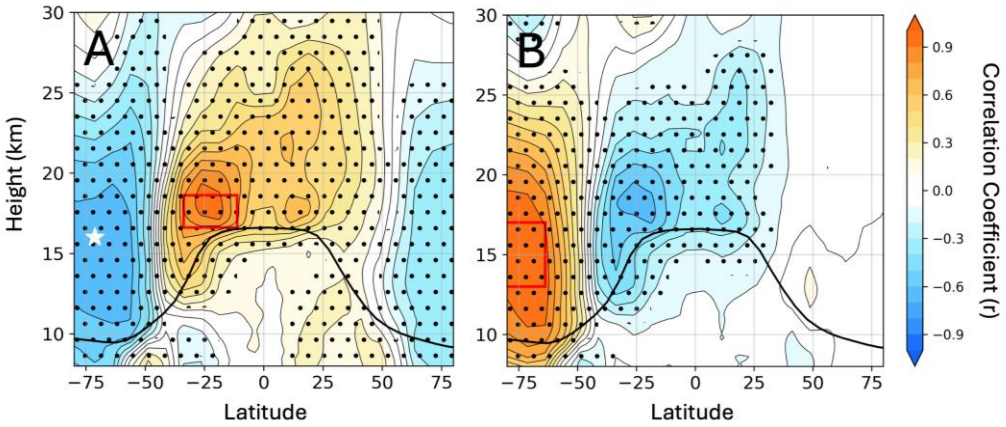

Figure 2: (A) Correlations between the detrended AWLS timeseries and the detrended temperature anomalies from 8 to 30 km. (B) Same as (A), but for the detrended temperature anomalies in the Antarctic lower stratospheric region from 63.7°S -90°S and 13-17 km. Stippling indicates statistically significant correlations. The climatological lapse-rate tropopause height is indicated by the thick black line. The white star shows the location used in Figs. 3 and 5.

Next, we use the circulation regression technique outlined in Section 2.5 to separate stratospheric changes associated with the AWLS timeseries from those that are not. Figure 3 illustrates this for one location in the Antarctic lower stratosphere (71.25°S, 16 km; white star in Fig. 2A), which we expect to be coupled to the AWLS via the SH-BDC. The observed temperature anomaly timeseries at this location (Fig. 3A) shows an insignificant change of -0.35 ± 1.11 K/decade. Regressing the detrended temperature at this region onto the detrended AWLS timeseries results in a regression coefficient of -2.73 K/K and a correlation coefficient of -0.66, revealing strong coupling between these regions. Multiplying this coefficient by the original AWLS timeseries produces the timeseries shown in Fig. 3B, which we interpret as representing circulation variability. This timeseries has a statistically significant change of -1.09 ± 0.9 K/decade. Figure 3C is the difference after removing covariability with the AWLS from the

observed temperature timeseries. This difference timeseries has a statistically significant positive trend and a smaller uncertainty (0.74 ± 0.64 K/decade).

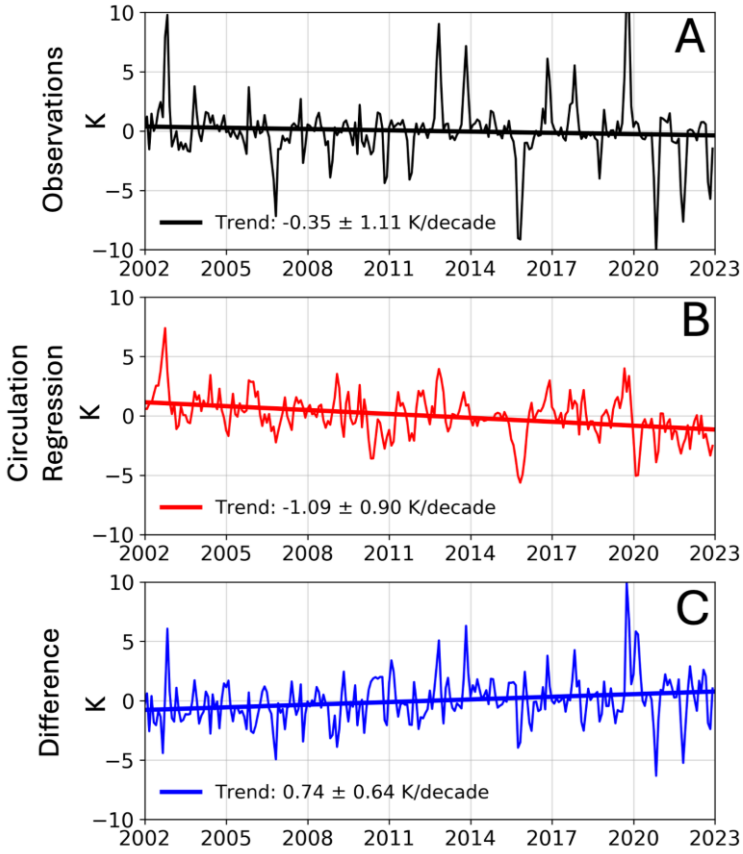

Figure 3: Example of the circulation regression technique applied to temperatures at a specific Antarctic lower stratosphere location (71.25°S, 16 km). (A) RO-observed temperature anomaly timeseries. (B) Circulation regression timeseries, obtained by multiplying the AWLS timeseries by the regression coefficient between the detrended temperature anomalies and the detrended AWLS timeseries. (C) The difference between the observed anomalies (A) and the circulation regression component (B), i.e., C = A – B.

The regression coefficient used reflects the interannual coupling between the AWLS and Antarctic, mediated by the SH-BDC. Wang et al. (2025) found that interannual variability of Antarctic lower stratospheric ozone is amplified due to ODSs. This occurs at least in part because interannual variability in the BDC can also influence the efficiency of ozone depletion by modulating polar vortex temperature and location (see Wang et al., 2025 for details). This enhanced ozone variability in turn affects the temperature variability. Figure S3 shows the ratio of the standard deviation in detrended temperature anomalies between 2002-2022 (ODS period) and 1955-1975 (pre-ODS period), based on ERA5 data for (A) January-April, (B) May–August, and (C) September–December. It reveals that Antarctic temperature variability during September-December in the ODS period can be up to ~100% higher, supporting Wang et al. (2025). This increased internal variability in both temperature and ozone during this period makes the detection of ozone recovery and its corresponding temperature response more challenging. Since the regression coefficient in the circulation regression is derived from

observed interannual variability during 2002-2022, it inherently accounts for the impact of dynamics, chemistry, and radiative interactions on interannual variability during the ODS period.

We now apply the circulation regression to temperatures in the UTLS from 8-30 km. Figure 4 presents the results: panel A shows the RO temperature changes from 2002-2022 (identical to Fig. 1A), panel B displays the temperature changes that are congruent with those in the AWLS region, and panel C illustrates the difference between panels A and B.

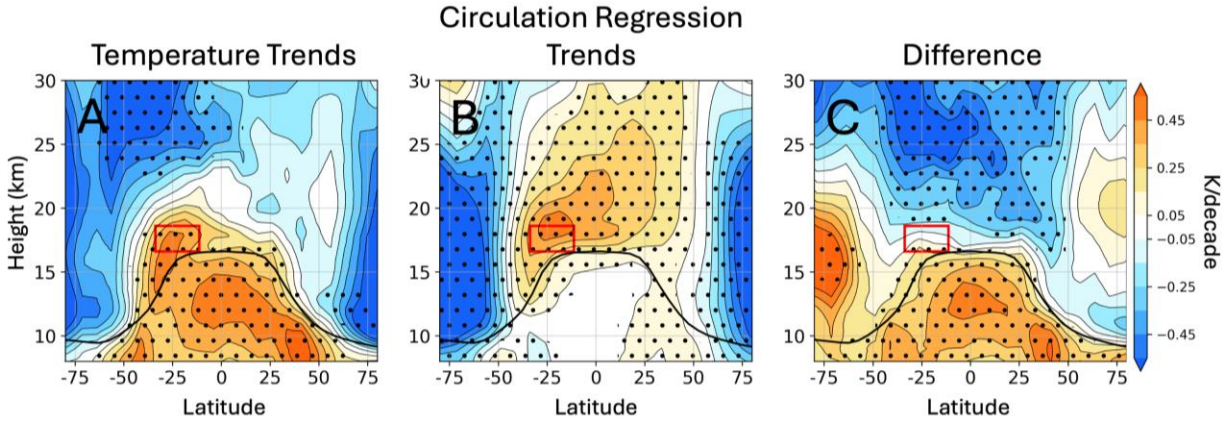

Figure 4: (A) The same as Fig. 1A. (B) Trends related to AWLS based on circulation regression. (C) Difference trend (i.e., A – B). Stippling in panels A and C indicates areas where trends are statistically significant, while in panel B, stippling shows regions where the regression coefficients from the circulation regression are statistically significant. The tropopause is indicated by the thick black line.

The changes related to the AWLS (Fig. 4B) exhibit a warming of the tropical lower stratosphere, which hugs the SH subtropical tropopause near the AWLS region, and strong cooling at high latitudes in both hemispheres. This pattern of temperature change in Fig. 4B is consistent with a slowdown of the lower-stratospheric BDC (Fu et al., 2019), characterized by reduced upwelling (i.e., less cooling) in the tropics and decreased downwelling (i.e., less warming) in the high latitudes. Because the linear trend of the AWLS timeseries is statistically significant (Fig. 1B), the trends in Fig. 4B are also statistically significant, as they are derived by multiplying the AWLS timeseries by the corresponding regression coefficients.

Figure 4C presents the temperature change that is not related to the AWLS timeseries, showing strong tropospheric warming and stratospheric cooling, which are the expected atmospheric temperature responses to increased GHGs. In addition, Fig. 4C reveals significant warming in the Antarctic lower stratosphere, a feature absent in the observed changes (Fig. 4A). This Antarctic lower stratospheric warming is a predicted consequence of ozone healing, as shown in chemistry-climate models, and is expected to peak between September-January near 16 km, mirroring the cooling seen during the ozone depletion era (Solomon et al., 2017; Randel et al., 2017; Fu et al., 2019).

The resemblance between the temperature trend pattern from circulation regression (Fig. 4B) and the expected BDC-driven temperature changes reflects our method of isolating these changes using regression coefficients based on interannual variability, which is largely

influenced by the BDC. In contrast, the difference panel in Fig. 4C aligns with the anticipated temperature response to GHG increases and Antarctic ozone recovery. The similarity of Fig. 4C to the expected GHG- and ozone-induced changes suggests that circulation variability is largely internal and has been effectively removed. This reinforces the interpretation that the changes in Fig. 4B are primarily due to the stratospheric circulation.

To test whether that the AWLS may alternatively be driven by radiative processes, we use the radiative transfer model described in Section 2.3 to estimate the impact of observed atmospheric composition changes on the lower stratospheric temperature (Keeling et al., 1976; Forster and Shine, 1997; Fu et al., 2015; Davis et al., 2016; Lan et al., 2022). Observed changes in radiatively active species, including GHGs, CFCs, and stratospheric O_3, and H_2O, are considered. The results indicate that in response to composition changes, the AWLS region should *cool* at a rate of -0.18 K/decade. Breaking this down by individual contributions, GHGs & CFCs contribute -0.072 K/decade to the total cooling, while stratospheric O_3 and stratospheric H_2O contribute -0.064, and -0.044 K/decade, respectively. While observed changes in stratospheric O_3 and H_2O are also influenced by circulation, the fact that radiative processes would lead to cooling suggests that the pronounced warming of the AWLS region is primarily driven by circulation changes. This strengthens confidence that the decadal variability associated with the AWLS is linked to the circulation trends.

3.2 Seasonality of Temperature Changes

A key finding from Fig. 4C is the warming of the Antarctic lower stratosphere consistent with ozone recovery after accounting for circulation variability. However, since Fig. 4 shows temperature changes based on anomalies from all months, it does not capture the strong seasonal dependence of ozone recovery. To address this, we apply the circulation regression separately for each month to derive the monthly-resolved circulation impact on temperature changes.

Figure 5A provides an example of the circulation regression applied to the temperature timeseries at a location in the Antarctic stratosphere (white star in Fig. 2A), like Fig. 3 but applied to the month of October. Observed temperature in October shows an insignificant cooling, with strong interannual variability (black line in Fig. 5A). This interannual variability is closely captured by the temperature derived from the circulation regression (red line in Fig. 5A), reflecting the strong temperature covariability between the AWLS region and Antarctica. Notably, interannual variability in the AWLS region and the Antarctic location are more strongly correlated during October than in most other months, with a correlation coefficient of -0.86 and a regression coefficient of -4.9 K/K. This is further illustrated in Fig. S4, which presents interannual correlation maps between the AWLS region and the UTLS for each month. Removing circulation variability from October temperature (blue line in Fig. 5A) strongly reduces interannual variability and reveals a statistically significant warming trend in the region. The results for ozone (Fig. 5B) will be discussed in Section 3.3.

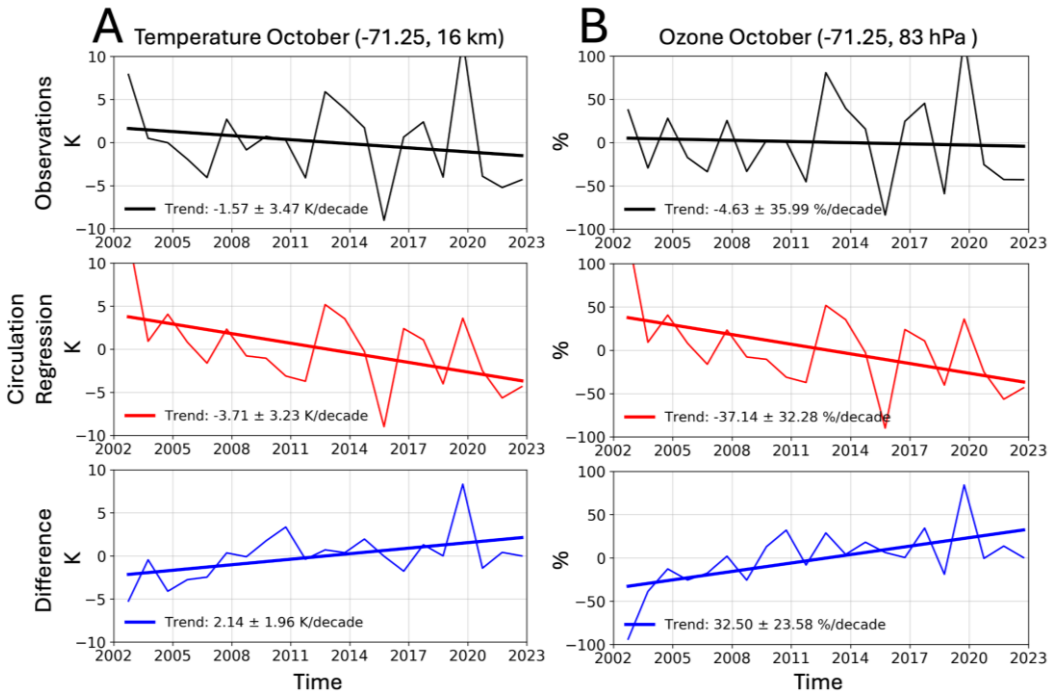

Figure 5: (Black) Timeseries and trends of observed (A) temperature at (71.25°S, 16 km) and (B) ozone at (71.25°S, 83 hPa) in October. (Red) Temperature and ozone timeseries and trends obtained from the monthly circulation regression. (Blue) The difference timeseries and trends after removing the circulation regression component from the observations.

Figure 6 displays temperature trends for 2002-2022 for each month from July-December and shows results from the monthly circulation regression applied to temperatures from 8-30 km, while Fig. S5 provides corresponding changes for January to June. Figure 6 row 1 reveals that tropospheric warming persists year-round, while stratospheric temperature changes depend strongly on season (Khaykin et al., 2017). Figure S6 presents the monthly AWLS timeseries and changes, indicating consistent warming in the AWLS region throughout the year, with peak warming occurring in October-November and the weakest warming observed in April-May (Ladstädter et al., 2023).

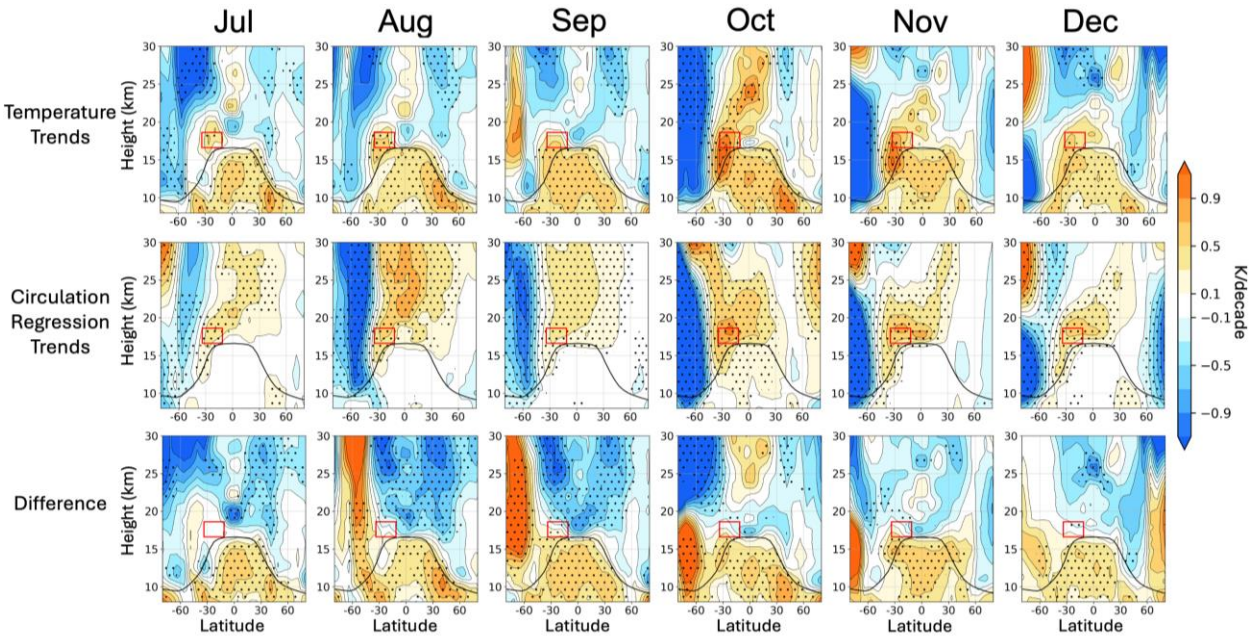

Figure 6: Monthly trends in temperature for the 2002-2022 period. Row 1 shows temperature trends from July to December. Row 2 shows the corresponding trends associated with AWLS based on the circulation regression. Row 3 shows difference trends (i.e., Row 1 minus Row 2). Stippling in rows 1 and 3 indicates areas where trends are statistically significant, while in row 2, stippling shows regions where the regression coefficients from the circulation regression are statistically significant. The climatological tropopause is indicated by the thick black line.

The second row of Fig. 6 shows corresponding temperature changes associated with the AWLS, obtained from the monthly circulation regression. Distinct patterns emerge depending on the month, highlighting both the seasonal variation in AWLS magnitude and its relationship to UTLS temperatures. The strongest dipolar coupling between the AWLS region and the Antarctic lower stratosphere occurs from October-December (row 2 of Fig. 6). This dipolar pattern during these months closely resembles the circulation-related temperature anomalies identified during the 2002 Antarctic SSW, as documented by Randel and Wu (2015, see their Fig. 9). Furthermore, the AWLS during January to April are linked to the Arctic stratosphere (row 2 of Fig. S5).

The third row of Fig. 6 presents temperature changes after removing AWLS-related circulation variability. Between August and September, the warming poleward of 50°S intensifies, peaking above 20 km and expanding to cover the polar cap by September. This poleward progression of Antarctic stratospheric warming follows the latitudinal shift of insolation during these months. This warming also descends in altitude, qualitatively aligning with the expected ozone recovery signal in temperature during this period (Solomon et al., 2017; Wang et al., 2025).

After removing AWLS-related changes, an Antarctic warming emerges during September-January (row 3 of Figs. 6 and S5), aligning with the seasonality of ozone recovery (see Sections 3.3; Fig. 7). Internal dynamical variability in the SH can hinder the ability to detect signatures of ozone recovery, particularly in October and November (WMO, 2022). However,

Fig. 6 suggests that removing the circulation effects associated with the AWLS reveals a temperature response consistent with the expected impact of ozone recovery.

Previous studies suggest that during the 21st century, the NH-BDC has slowed more than the SH-BDC above 25 km (Ploeger and Garny, 2022; Dubé et al., 2025). While our circulation regression analysis does not quantify the relative magnitude of the slowdown between the NH and SH-BDC, our results also support a slowdown of the NH-BDC for 2002-2022 (Fig. 4B and middle panels in Fig. S5 for January – April). Furthermore, Figs. 6 and S5 indicate that the AWLS from January to May is largely linked to the NH-BDC slowdown, while from June to December, it is linked to the SH-BDC slow down. As a result, the SH-BDC and NH-BDC slowdown contributes to the AWLS roughly by 0.27 ± 0.27 K/decade and 0.13 ± 0.13 K/decade, respectively, based on Fig. S6. The former drives the dynamically induced cooling in the Antarctic lower stratosphere.

3.3 Ozone Changes

In this section, we investigate the role of AWLS-related circulation variability in observed stratospheric ozone changes from 2002-2022. Figure 5B provides an example of applying the circulation regression to October ozone concentrations in the Antarctic stratosphere at -71.25°S and 83 hPa. Ozone variations are shown as percent anomalies relative to the 2002-2022 monthly climatology, highlighting changes in the lower stratosphere. The black line in Fig. 5B represents observed ozone variability, revealing an insignificant change of -4.63 ± 35.99 %/decade. This result is consistent with Figure 4-16 of the WMO Ozone Assessment Report (WMO, 2022), showing little October total ozone trends over 60°S-90°S since 2000. Regressing interannual October ozone variability at this location onto the detrended AWLS timeseries suggests a strong coupling, with a regression coefficient of -49 %/K (r = -0.83). Notably, the interannual variation of observed ozone (black line in Fig. 5B) closely follows that of circulation variability (red line in Fig. 5B), which represents the AWLS timeseries multiplied by the regression coefficient. After removing AWLS-related ozone variability, the resulting difference timeseries (blue line in Fig. 5B) reveals a significant increase in ozone of 32.5 ± 23.58 %/decade.

The coupling between AWLS temperature and Antarctic ozone (e.g., Fig. 5B) can be largely explained by the SH-BDC. Since most high-latitude ozone originates in the lower-latitude stratosphere and is transported poleward by the BDC, a slowdown in the SH-BDC leads to reduced Antarctic ozone concentrations (e.g., Dobson, 1956; Garcia and Solomon, 1983; Perliski et al., 1989; Shephard, 2007; Orbe et al., 2020). During the ODS period, a weakened SH-BDC further decreases Antarctic ozone by inducing colder Antarctic stratospheric vortices, enhancing chemical ozone depletion and contributing to greater Antarctic ozone interannual variability (Wang et al., 2025). Due to elevated ODS concentrations, a slowdown of the SH-BDC reduces Antarctic ozone through both reduced transport and increased chemical loss due to lower temperatures.

We now apply the circulation regression to monthly ozone changes, similar to those applied to temperature in Fig. 6. The first row of Fig. 7 shows observed changes from July-December for 2002-2022, while changes from January-June are shown in Fig. S7. Observations indicate clear signs of Antarctic ozone healing in September (Solomon et al., 2016); however,

changes from October-December primarily show a decline. This decline may result from strong circulation variability, sensitivity to additional forcings not accounted for in the models, and/or observational uncertainties (Solomon et al., 2016; Chipperfield et al., 2017; Kuttippurath and Nair, 2017; Montzka et al., 2018; Stone et al., 2021; Yook et al., 2022; Solomon et al., 2022; Solomon et al., 2023; Kessenich et al., 2023; Villamayor et al., 2023). In this study, we focus on the role of circulation variability.

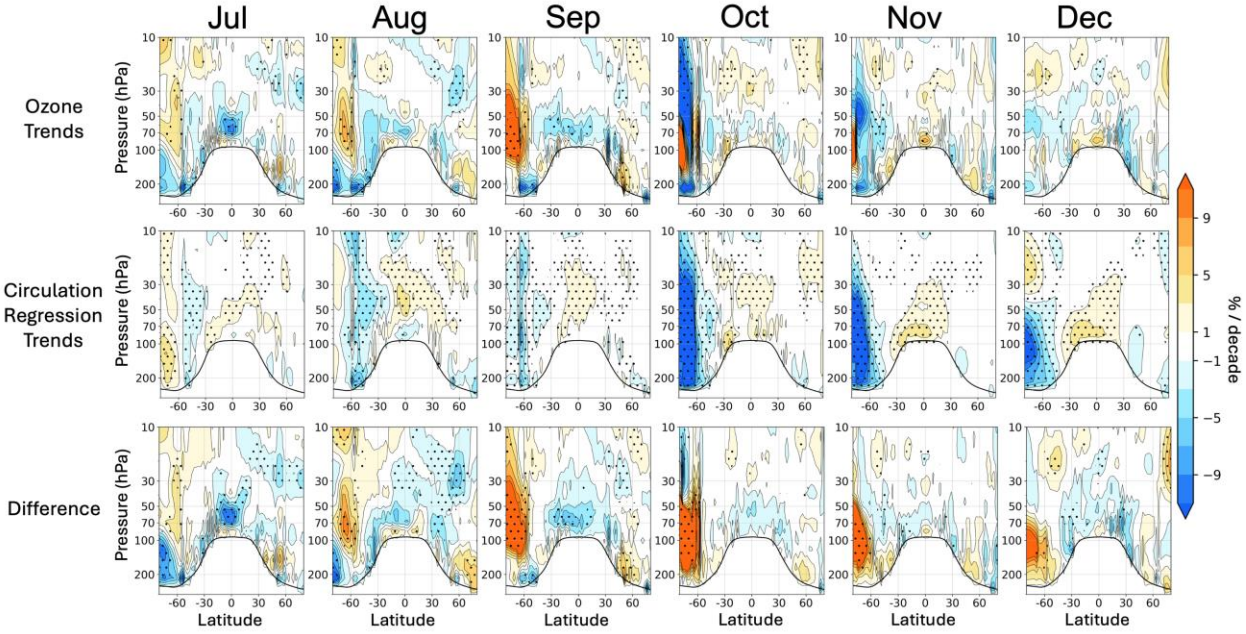

Figure 7: As Fig. 6, but for trends in SWOOSH ozone concentration as percent anomaly relative to the 2002-2022 climatology.

The second row of Fig. 7 presents the impact of AWLS-related circulation variability on ozone changes. Between October-December, circulation variability decreases Antarctic ozone trends while enhancing positive trends in the tropical lower stratosphere. This dipolar pattern between the tropical and Antarctic lower stratosphere is consistent with a slowdown of the SH-BDC.

The third row of Fig. 7 shows ozone changes after removing circulation-driven variability, highlighting a significant increase in Antarctic ozone starting in August. Similar to the temperature changes (row 3 of Fig. 6), the observed poleward expansion of the ozone recovery in the Antarctic stratosphere follows the seasonal shift of insolation from August to September. The ozone healing also descends throughout austral spring into summer, aligning with the mean downward motion of polar air due to the BDC, which is an expected feature of ozone healing (Solomon et al., 2017). Overall, the third rows of Figs. 6 and 7 suggest that removing AWLS-related changes reveals increases in both temperature and ozone, consistent with the expected effects of ozone recovery (Solomon et al., 2016; Solomon et al., 2017; Calvo et al., 2017).

While Fig. 7 focuses on monthly ozone changes to identify Antarctic ozone recovery, Fig. 8 shows changes calculated from monthly anomalies over all months. In Fig. 8A, annual

ozone changes from SWOOSH indicate small, insignificant trends in Antarctic ozone poleward of 75°S. Fig. 8B displays the annual mean ozone changes associated with AWLS-related circulation variability. Consistent with the monthly ozone analysis, ozone concentrations increase in the tropical lower stratosphere and decrease in the Antarctic, reflecting changes in the SH-BDC. Finally, Fig. 8C shows ozone changes after removing the circulation variability, revealing a widespread increase in Antarctic ozone.

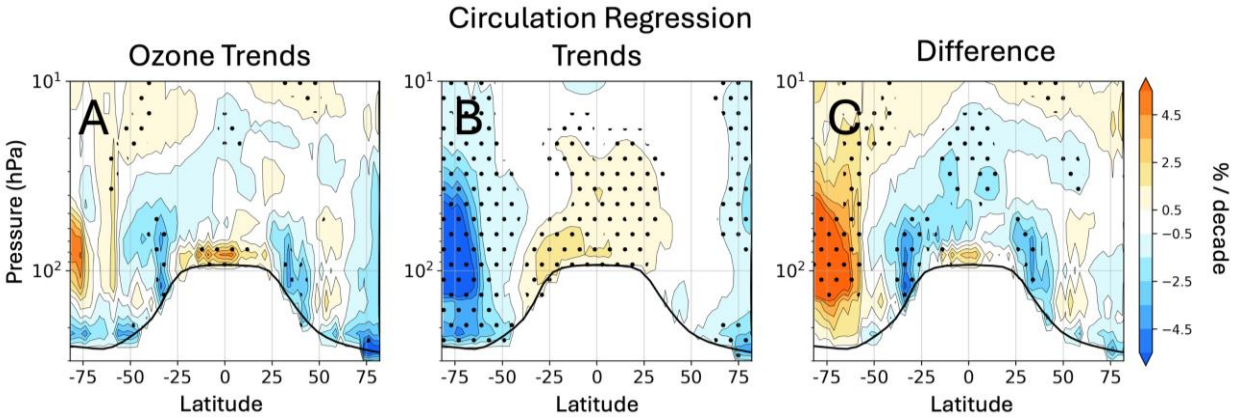

Figure 8: As Fig. 4, but for trends in SWOOSH ozone concentration as percent anomaly relative to the 2002-2022 climatology.

3.4 Comparison with Model Simulations

Figure 9A presents ensemble mean temperature changes for 2002-2022 from the CESM1-WACCM 10-member simulations (Zambri et al., 2021). Averaging over the 10 members to obtain the ensemble mean largely mutes the effect of internal variability and provides an estimate of the WACCM simulated forced response over this period. The key differences between the ensemble mean and the observed temperature trend shown in Fig. 1A are the minimal warming of the AWLS region and the pronounced warming of the Antarctic lower stratosphere in the simulations (c.f., Fig. 1A and Fig. 9A). Similarly, a comparison of ozone changes reveals a notable difference, with the ensemble mean showing a significant recovery of Antarctic ozone (c.f., Fig. 8A and Fig. 9B). Given the influence of internal variability, we do not expect strong agreement between observed and simulated ensemble mean changes (see Section 4.7).

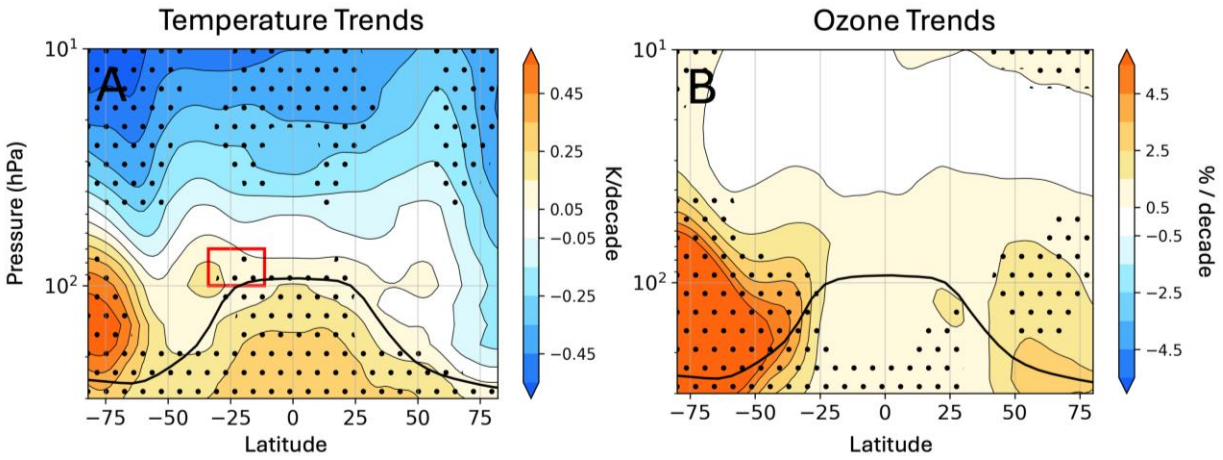

Figure 9: The 10-member ensemble mean of WACCM simulations for (A) temperature and (B) ozone trends for 2002-2022. Stippling and the thick black line follow the same conventions as in Fig. 1A.

Removing circulation variability from observed temperature changes reveals strong warming in the Antarctic lower stratosphere while minimizing warming in the tropical lower stratosphere (see Fig. 4C). Similarly, removing circulation variability from ozone changes displays an obvious recovery of Antarctic ozone (Fig. 8C). Overall, in both temperature and ozone, accounting for AWLS-related stratospheric circulation results in a better agreement between observed and WACCM simulated changes (c.f., 4C and 9A for temperature, and 8C and 9B for ozone). Removing the circulation variability from ozone changes also slightly exacerbates the observed decreases in tropical ozone.

The circulation-adjusted ozone trends in Fig. 8C also show significant declines in the subtropical lower stratosphere of both hemispheres, as well as in the tropical region between~15-40 hPa—different from the pattern in Fig. 9b. Removing the circulation variability from observed ozone changes thus slightly exacerbates the observed decreases in tropical ozone. These declines persist throughout the year (Figs. 7 and S7), especially from February to June, even before applying the circulation adjustment. Future research is needed to understand why ozone levels are decreasing in these regions despite the reduction in ODS.

Figure S8 (S9) shows the monthly temperature (ozone) changes from the WACCM ensemble mean simulations. Like the monthly temperature (ozone) changes after removing circulation variability in the third row of Fig. 6 (Fig. 7), the WACCM simulations show a seasonally dependent change in Antarctic lower-stratospheric temperature (ozone), which peaks from November–February (October-February). Note that the strongest warming and ozone recovery in this region from the WACCM simulations lag the signals seen in observation (the third row of Figs. 6 and 7) by 1-2 months. This may be due to known model biases that delay the breakdown of the SH polar vortex (Butchart et al., 2011; Calvo et al., 2017; Lawrence et al., 2022).

4 Discussion & Sensitivity Analysis

Section 3 suggests that stratospheric circulation changes are a primary driver of observed AWLS and Antarctic lower stratospheric cooling, which also obscure ozone recovery signals in certain months. Removing these circulation effects eliminates the anomalous warming of the SH subtropical lower stratosphere and reveals Antarctic lower stratospheric warming and ozone recovery. Below we discuss these findings in a broader context.

4.1 Sensitivity to Start and End Dates

Previous studies suggest that excluding years with extreme dynamical variability, or unanticipated forcings (e.g., wildfire, volcanic activity) may help detect ozone recovery (Bernath et al., 2022; Yook et al., 2022; Solomon et al., 2022; Solomon et al., 2023; Stocker et al., 2021; Wang et al., 2023; Zhang et al., 2024; Stocker et al., 2024). To evaluate the circulation regression's ability to isolate circulation effects, we test its sensitivity to different start and end dates, focusing on October-December. If the method is robust, the changes after removing circulation effects should remain similar regardless of the start and end dates.

Figure 10 presents the temperature (left) and ozone (right) results for October across the periods 2005-2018, 2003-2022, and 2002-2021, in comparison to the full period of 2002-2022. October Antarctic ozone exhibits large interannual variability and is highly influenced by strong dynamical activity (WMO, 2022). Results for November and December are displayed in Figs. S10 and S11. The 2005-2018 period was recently considered in Wang et al. (2025) to investigate Antarctic ozone recovery because of minimal impact of extreme dynamics, wildfires, and volcanoes. Interestingly, the observed annual mean AWLS change over this period is 0.1 K/decade, which matches the WACCM ensemble mean warming of 0.1 K/decade there (Fig. 9A), suggesting a minimal circulation variability impact. While 2005-2018 circulation variability has some negative impact on October Antarctic temperature and ozone, its impacts are minimal in November and December (Figs. S10 & S11) (Wang et al., 2025). Although observed Antarctic

temperature and ozone changes remain positive in these months, the October increases become more pronounced after accounting for circulation effects (Fig. 10).

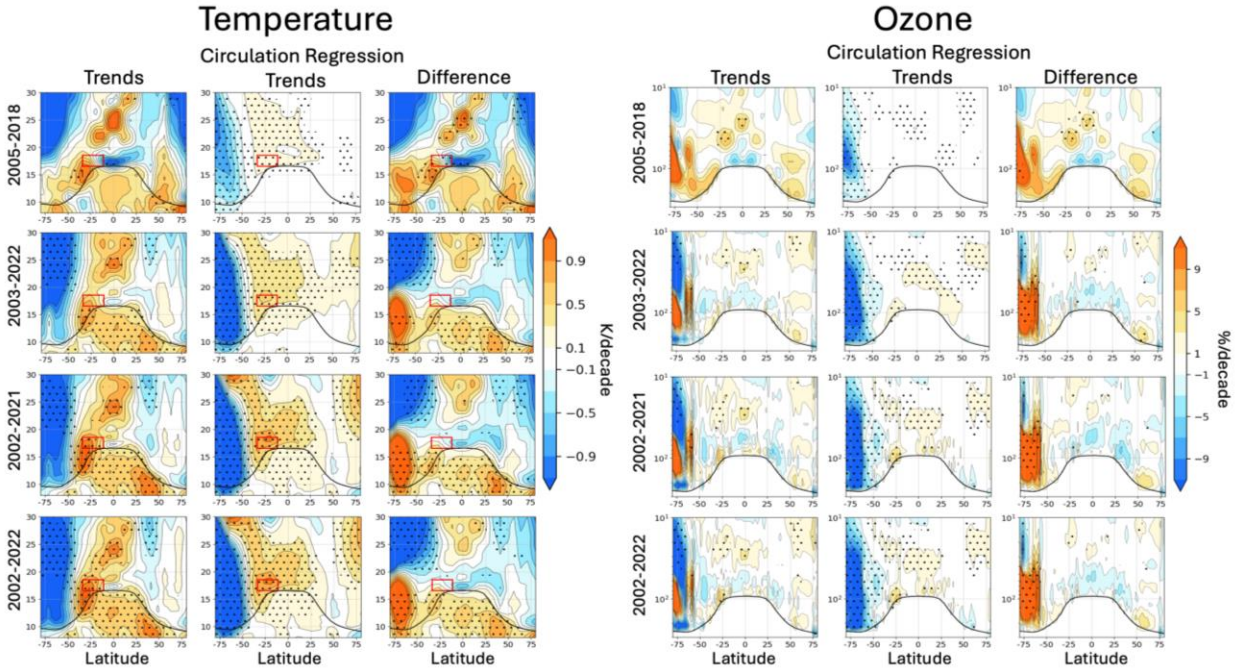

Figure 10: Left (Right): Same as Fig. 4 (8) for temperature (ozone) trends but for October during 2005-2018, 2003-2022, and 2002-2021.

For the periods 2003-2022 (excluding the 2002 Antarctic SSW) and 2002-2021 (omitting 2022 to avoid the impact of the Hunga-Tonga eruption), comparisons with the full period 2002-2022 reveal minimal sensitivity to the choice of the start and end years. After removing circulation variability, all periods consistently display Antarctic lower stratospheric warming, and ozone increases--key features of long-term ozone recovery. However, some quantitative differences between 2005-2018 and the other periods remain evident, even after removing circulation variability, potentially arising from variations in external forcing, observational uncertainties, and residual effects of circulation variability.

4.2 ERA5 Residual Circulation Changes

If the AWLS is due to changes in the BDC, this should be reflected in residual circulation changes over recent decades. Changes in the ERA5 residual stream function are shown in Fig S12. Climatological values of the residual stream function are negative in the SH, yet changes show large positive values in this region, suggesting a weakening of the SH-BDC. Note that estimates of the residual circulation changes might not be well constrained in reanalysis datasets and can vary between products (Ploeger and Garny, 2022; SPARC, 2022). Yet, the different lines of evidence from the circulation regression analysis, radiative transfer calculations, and ERA5 residual stream function changes all point to a dynamically induced AWLS, which can be interpreted as a weakening of the BDC, especially in the SH. Figure S12 also indicates a weakening of the NH-BDC.

642 4.3 Relevance to Zonal Wind Changes
643
644 Perturbations to the lower-stratospheric temperature gradient associated with the
645 identified circulation variability must align with zonal wind changes through thermal wind
646 balance. In Fig. S13, we partition ERA5 zonal wind changes into those related to the AWLS
647 timeseries and those not related to it by applying the circulation regression to monthly ERA5
648 zonal wind anomalies (see Section 2.5). The ERA5 zonal wind changes (Fig. S13A) show that
649 the stratospheric jet has strengthened in both hemispheres from 2002-2022, with the strongest
650 intensification near 50°S-60°S. The circulation regression changes show that the AWLS is
651 associated with significant strengthening of the polar stratospheric zonal wind in both
652 hemispheres (Fig. S13B). Removing these changes results in small negative and statistically
653 insignificant decadal changes in polar stratospheric zonal wind (Fig. S13C), suggesting that the
654 observed stratospheric wind trends are mostly related to the AWLS.
655
656 4.4 The Role of the Southern Annular Mode
657
658 Changes in the strength and position of the SH stratospheric jet can be understood as
659 variability of the Southern Annular Mode (SAM) (Thompson & Wallace, 2000; Fogt and
660 Marshall, 2020). This raises the question of whether the circulation variability we identify here is
661 simply a reflection of variability in the SAM. To examine this, we apply an adapted version of
662 the circulation regression to monthly temperature anomalies, by replacing the AWLS timeseries
663 with a SAM index (see Section 2.1 for its definition). The results are shown in Fig. S14. Notably,
664 the AWLS region exhibits a local maximum response to SAM (Fig. S14B), further highlighting
665 its dynamic coupling with the Antarctic lower stratosphere. While the pattern of stratospheric
666 temperature changes associated with the SAM (Fig. S14B) closely resembles the circulation
667 regression results in Fig. 4B, the SAM-related warming in the region of the AWLS is only 0.13 ±
668 0.1 K/decade, which is ~1/3 of the 0.4±0.33 K/decade warming trend in the AWLS region (see
669 Fig. 1B). This may be partly because the SAM closely tracks the polar vortex strength, which has
670 been strengthened by circulation-driven cooling of the Antarctic stratosphere and weakened by
671 warming due to externally driven ozone healing, leading to a partial cancellation and smaller net
672 changes in the SAM.
673
674 4.5 Sensitivity to Box Location as Key Center of BDC Variability
675
676 The circulation regression technique (Section 2.5) identified the AWLS region as a key
677 center of SH-BDC variability (Fig. 2). While both the SH- and NH-BDC influence the tropical
678 lower stratosphere, using both the AWLS timeseries and the temperature anomaly timeseries of
679 the NH subtropical lower stratospheric (see red box in Fig. S2A) has little effect on the results of
680 Fig. 4 (not shown). This is because the AWLS timeseries as a good proxy for the NH BDC
681 during January – March, when NH BDC dominates (see Fig. S5). Notably, the detrended AWLS
682 timeseries correlates with its NH counterpart at $r = 0.60$.
683
684 Figure S15 further tests the sensitivity of our results by replacing the AWLS region box
685 with a more conventional "tropical box" spanning 26.25°S to 26.25°N at the same height (Fig.
686 15). While this approach still tracks stratospheric circulation (Fig. S15B), it captures less AWLS
687 warming. Difference changes (Fig. S15C) recover weak, insignificant Antarctic lower

stratospheric warming, and still exhibit strong SH subtropical warming. These results suggest that while the tropical box captures part of variability associated with the stratospheric circulation, it is less indicative of the SH-BDC variability than the selected AWLS region. Notably, the difference change patterns for the NH in Figs. 4 and S13 are nearly identical, indicating that the AWLS region also effectively captures the slowdown of the NH-BDC well (Figs. S5 and S12). Using a "tropical box" spanning 18.75°S to 18.75°N yields very similar results to those in Fig. S15, though the coupling with the poles becomes even weaker.

4.6 Impact of Observational Errors on Circulation Regression Analysis

In the circulation regression analysis, trends unrelated to the circulation are obtained by subtracting circulation variability from the original anomalies. A relevant question is how observational errors affect the trend uncertainty interval of this difference. Suppose the observational errors for the target anomalies and AWLS timeseries are denoted as σ_a and σ_{AWLS}, respectively. The observational error in the difference is then given by $[\sigma_a^2 + (m_{ij}\,\sigma_{AWLS})^2]^{1/2}$, where m_{ij} is the regression coefficient. This indicates that the observational errors in the difference, which incorporate errors from both the target anomalies and the AWLS timeseries, are larger than those in the original anomalies and circulation variability. However, the trend uncertainty interval of the difference, which is due to both observational errors and interannual variability, remains smaller than that of the original anomalies (Figs. 3 and 5). This is because the trend uncertainty is dominated by interannual variability. Since removing circulation variability substantially reduces interannual variability in the difference, it results in a smaller trend uncertainty interval (Figs. 3 and 5). Even if the change in the AWLS region for a given month is small and statistically insignificant (Fig. S6), it still significantly contributes to the circulation regression analysis by reducing interannual variability in the difference, thereby narrowing its trend uncertainty interval.

4.7 Circulation Regression Applied to WACCM Simulations

Figure S16A shows temperature changes from 10 individual WACCM ensemble members over 2002-2022. While Antarctic lower-stratospheric temperature changes vary greatly among members, all members simulate similar weak warming in the AWLS region (ensemble mean: 0.1 K/decade). Since QBO and ENSO effects are removed, these differences primarily reflect internal BDC variability. Figure S16B shows changes related to each member's AWLS timeseries using circulation regression. Fig. S16C presents the difference changes after removing AWLS-related processes. The similarity between trend patterns in Figs. S16A and S16C indicates that the circulation regression approach is ineffective for model simulations.

Figure S17 compares simulated and observed R^2 between detrended monthly temperature anomalies in the Antarctic lower stratosphere and UTLS temperatures. Observations show a strong coupling between the Antarctic and AWLS region ($R^2 \sim 0.35$), whereas simulations

exhibit a much weaker relationship (R^2~ 0.15) across all ensemble members. This suggests that the circulation regression is ineffective for this model's simulations.

4.8 Cause of BDC Changes

Model simulations suggest that two key external drivers of 21st-century BDC changes are rising GHG concentrations and Antarctic ozone recovery (McLandress et al., 2010; Garny et al., 2011; McLandress et al., 2011; Lin and Fu, 2013; Garfinkel et al., 2017; Abalos et al., 2019; Abalos et al., 2020; Abalos et al., 2021; Ivanciu et al., 2022). Increasing GHG levels are expected to accelerate the BDC, causing cooling in the tropical lower stratosphere and warming at the poles—opposite to the observed trends (Fig. 1A). In contrast, Antarctic ozone recovery is expected to warm the lower stratosphere over Antarctica, weakening the SH equator-to-pole temperature gradient and inducing a forced slowdown of the SH-BDC (Polvani et al., 2018; Abalos et al., 2019; Polvani et al., 2019; Ladstädter et al., 2023). However, this simulated slowdown relies on a significant increase in Antarctic ozone concentration, which would warm the Antarctic. Since such strong increases are absent in observed ozone and temperature changes, the results presented here do not support a forced slowdown of the SH-BDC due to Antarctic ozone recovery.

The WACCM simulation indicates a forced warming of 0.1 K/decade and a radiative component of -0.12 K/decade in the AWLS region, resulting in a forced dynamic component of 0.22 K/decade. Observations, however, indicate a total warming of 0.4 K/decade, with a radiative component of -0.18 K/decade, implying a dynamic component of 0.58 K/decade. This implies that the dynamic component due to internal variability is 0.36 K/decade. Consequently, if we have confidence in the model-simulated forced changes, the 0.4 K/decade (Fig. 1B) used in our analysis should largely reflect internal variability.

5 Conclusions

The RO climate record allows for a detailed study of 21st century stratospheric temperature changes (Khaykin et al., 2017; Shannguan et al., 2019; Steiner et al., 2020b; Mitchell et al., 2020; Vergados et al., 2020; Gleisner et al., 2022, Ladstädter et al., 2023; Zolghadrshojaee et al., 2024). While models predict widespread stratospheric cooling, RO observations for 2002-2022 show anomalous warming in the SH subtropical lower stratosphere, referred to here as the AWLS. Partitioning temperature changes into those related to the AWLS (Fig. 4B) and those that are not (Fig. 4C) reveals the influence of stratospheric circulation on temperature changes, distinguishing them from changes driven by rising GHG levels and ozone recovery. This approach remains robust to choices of different time periods (Fig. 10, S10, and S11), reflecting the importance of circulation changes from interannual to decadal timescales for polar temperatures. Seasonal analysis suggests that circulation variability has the strongest impact from October-December. Furthermore, radiative transfer calculations suggest that composition changes alone would lead to cooling in the AWLS region, providing further evidence that warming in this region is circulation driven. Changes in the ERA5 residual stream function also reinforce the evidence for dynamical warming in the AWLS region for 2002-2022. Our findings suggest that the circulation changes identified in this study are largely linked to internal variability rather than to increases in greenhouse gases or reduction in ODSs

Following the pronounced 20th century ozone depletion, stratospheric ozone concentrations are expected to recover in the 21st century due to the reduction of ODSs (Solomon et al., 2016; WMO, 2022). Detecting robust Antarctic ozone healing is crucial for demonstrating the effectiveness of the Montreal Protocol and its role in mitigating ozone depletion (Newman et al., 2006; Montzka et al., 2018; Barnes et al., 2019; Rigby et al., 2023). While Antarctic ozone healing has been observed during September, October-December ozone healing is less robust (Fig. 7). Our findings indicate that the SH-BDC slowdown linked to the AWLS reduces Antarctic ozone concentrations. This is because a weakened SH-BDC reduces poleward ozone transport and creates colder conditions favorable for the chemical depletion of ozone within the Antarctic polar vortex. Our results show that October-December Antarctic ozone recovery would be apparent in observations in the absence of recent circulation influences, consistent with previous studies (Solomon et al., 2016). Overall, we link two previously unconnected discrepancies between models and observations: the AWLS and the weaker-than-expected October-December Antarctic ozone healing.

Future stratospheric climate change will impact surface climate via dynamical and radiative stratosphere-troposphere coupling, thus understanding recent changes in stratospheric dynamics is important (e.g., Butchart, 2014; Haynes et al., 2021). However, constraining the BDC changes over recent decades is difficult, as most BDC metrics are not directly observable and must be inferred from a combination of temperature observations, trace gas measurements, models, and/or reanalysis products (Fu et al., 2010; 2015; 2019; Stiller et al., 2012; Mahieu et al., 2014; Abalos et al., 2015; Stiller et al., 2017; Ploeger and Garny, 2022; Diallo et al., 2021; SPARC, 2022). This study examines signatures of stratospheric circulation change using temperature provided by high vertical resolution RO data. While temperature is advantageous for studies of BDC change as it is directly observable, analyses using temperature are hindered by the fact that temperature is influenced by both the circulation and radiative processes. This study also calls for further research to investigate the root cause of recent stratospheric circulation changes identified here, which will help reduce uncertainties regarding future changes in stratospheric temperature, composition, and ultimately surface climate.

Acknowledgments

AS and QF were funded by NASA FINESST Grant 80NSSC22K1438 and NSF Grant AGS-2202812. Additional funding was provided by the Calvin Professorship in Atmospheric Sciences. AS's research benefits greatly by attending the GNSS Remote Sensing Colloquium, June 5-16, 2023, in Boulder, Colorado. SS and PW acknowledge support by NSF Grants AGS-2128617 and 2316980. Work by SP was supported by the Regional and Global Model Analysis Program of the Office of Science as part of the PCMDI Project and was performed under the auspices of the U.S. Department of Energy by Lawrence Livermore National Laboratory under Contract DE-AC52-07NA27344. We would like to acknowledge high-performance computing support from Cheyenne (doi:10.5065/D6RX99HX) provided by NCAR's Computational and Information Systems Laboratory, sponsored by the National Science Foundation, for part of the analyses presented in this study and for data management, storage, and preservation. This work was partially completed by the NASA-Aura-ACMAP Science Team under Grant

80NSSC23K1143. We thank Drs. Joel Thornton and Pieternel Levelt for valuable discussions. We also thank that the processing of the monthly RO record was done by Jon Starr of NCAR.

Open Research

Monthly RO used in this manuscript will be made available on Zotero by the time of publication of this manuscript. SWOOSH data is made available by NOAA. Software used to create figures will be made public on Aodhan Sweeney's github. RO data comes from the CDAAC website and SWOOSH data is made available by NOAA's Chemical Science Laboratory. Monthly ERA5 data comes from ECMWF's climate data store.

Conflict of Interest

The authors declare no conflicts of interest relevant to this study.

References

Abalos, M., Legras, B., Ploeger, F., & Randel, W. J. (2015). Evaluating the advective Brewer-Dobson circulation in three reanalyses for the period 1979–2012. *Journal of Geophysical Research: Atmospheres*, *120*(15), 7534–7554. https://doi.org/10.1002/2015JD023182

Abalos, M., Polvani, L., Calvo, N., Kinnison, D., Ploeger, F., Randel, W., & Solomon, S. (2019). New Insights on the Impact of Ozone-Depleting Substances on the Brewer-Dobson Circulation. *Journal of Geophysical Research: Atmospheres*, *124*(5), 2435–2451. https://doi.org/10.1029/2018JD029301

Abalos, M., Orbe, C., Kinnison, D. E., Plummer, D., Oman, L. D., Jöckel, P., et al. (2020). Future trends in stratosphere-to-troposphere transport in CCMI models. *Atmospheric Chemistry and Physics*, *20*(11), 6883–6901. https://doi.org/10.5194/acp-20-6883-2020

Abalos, M., Calvo, N., Benito-Barca, S., Garny, H., Hardiman, S. C., Lin, P., et al. (2021). The Brewer–Dobson circulation in CMIP6. *Atmospheric Chemistry and Physics*, *21*(17), 13571–13591. https://doi.org/10.5194/acp-21-13571-2021

Aquila, V., Swartz, W. H., Waugh, D. W., Colarco, P. R., Pawson, S., Polvani, L. M., & Stolarski, R. S. (2016). Isolating the roles of different forcing agents in global stratospheric temperature changes using model integrations with incrementally added single forcings. *Journal of Geophysical Research: Atmospheres*, *121*(13), 8067–8082. https://doi.org/10.1002/2015JD023841

Ball, W. T., Alsing, J., Staehelin, J., Davis, S. M., Froidevaux, L., & Peter, T. (2019). Stratospheric ozone trends for 1985–2018: sensitivity to recent large variability. *Atmospheric Chemistry and Physics*, *19*(19), 12731–12748. https://doi.org/10.5194/acp-19-12731-2019

Banerjee, A., Fyfe, J. C., Polvani, L. M., Waugh, D., & Chang, K.-L. (2020). A pause in Southern Hemisphere circulation trends due to the Montreal Protocol. *Nature*, *579*(7800), 544–548. https://doi.org/10.1038/s41586-020-2120-4

Barnes, P. W., Williamson, C. E., Lucas, R. M., Robinson, S. A., Madronich, S., Paul, N. D., et al. (2019). Ozone depletion, ultraviolet radiation, climate change and prospects for a sustainable future. *Nature Sustainability*, *2*(7), 569–579. https://doi.org/10.1038/s41893-019-0314-2

Bernath, P., Boone, C., & Crouse, J. (2022). Wildfire smoke destroys stratospheric ozone. *Science*, *375*(6586), 1292–1295. https://doi.org/10.1126/science.abm5611

Brewer, A. W. (1949). Evidence for a world circulation provided by the measurements of helium and water vapour distribution in the stratosphere. *Quarterly Journal of the Royal Meteorological Society*, *75*(326), 351–363. https://doi.org/10.1002/qj.49707532603

Butchart, N. (2014). The Brewer-Dobson circulation. *Reviews of Geophysics*, *52*(2), 157–184. https://doi.org/10.1002/2013RG000448

Calvo, N., Garcia, R. R., Randel, W. J., & Marsh, D. R. (2010). Dynamical Mechanism for the Increase in Tropical Upwelling in the Lowermost Tropical Stratosphere during Warm ENSO Events. *Journal of the Atmospheric Sciences*, *67*(7), 2331–2340. https://doi.org/10.1175/2010JAS3433.1

Calvo, N., R. R. Garcia, and D. E. Kinnison (2017), Revisiting Southern Hemisphere polar stratospheric temperature trends in WACCM: The role of dynamical forcing, *Geophys. Res. Lett.*, 44, 3402–3410, doi:10.1002/2017GL072792.

Chipperfield, M. P., Bekki, S., Dhomse, S., Harris, N. R. P., Hassler, B., Hossaini, R., et al. (2017). Detecting recovery of the stratospheric ozone layer. *Nature*, *549*(7671), 211–218. https://doi.org/10.1038/nature23681

Chipperfield, M. P., & Bekki, S. (2024). Opinion: Stratospheric ozone – depletion, recovery and new challenges. *Atmospheric Chemistry and Physics*, *24*(4), 2783–2802. https://doi.org/10.5194/acp-24-2783-2024

Clem, K. R., Renwick, J. A., & McGregor, J. (2017). Relationship between eastern tropical Pacific cooling and recent trends in the Southern Hemisphere zonal-mean circulation. *Climate Dynamics*, *49*(1), 113–129. https://doi.org/10.1007/s00382-016-3329-7

Cordero, R. R., Feron, S., Damiani, A., Redondas, A., Carrasco, J., Sepúlveda, E., et al. (2022). Persistent extreme ultraviolet irradiance in Antarctica despite the ozone recovery onset. *Scientific Reports*, *12*(1), 1266. https://doi.org/10.1038/s41598-022-05449-8

Davis, S. M., Rosenlof, K. H., Hassler, B., Hurst, D. F., Read, W. G., Vömel, H., et al. (2016). The Stratospheric Water and Ozone Satellite Homogenized (SWOOSH) database: a long-term database for climate studies. *Earth System Science Data*, *8*(2), 461–490. https://doi.org/10.5194/essd-8-461-2016

Dessler, A. E., Schoeberl, M. R., Wang, T., Davis, S. M., & Rosenlof, K. H. (2013). Stratospheric water vapor feedback. *Proceedings of the National Academy of Sciences*, *110*(45), 18087–18091. https://doi.org/10.1073/pnas.1310344110

Dhomse, S. S., Kinnison, D., Chipperfield, M. P., Salawitch, R. J., Cionni, I., Hegglin, M. I., et al. (2018). Estimates of ozone return dates from Chemistry-Climate Model Initiative simulations. *Atmospheric Chemistry and Physics*, *18*(11), 8409–8438. https://doi.org/10.5194/acp-18-8409-2018

Diallo, M., Ern, M., & Ploeger, F. (2021). The advective Brewer–Dobson circulation in the ERA5 reanalysis: climatology, variability, and trends. *Atmospheric Chemistry and Physics*, *21*(10), 7515–7544. https://doi.org/10.5194/acp-21-7515-2021

Ding, Q., & Fu, Q. (2018). A warming tropical central Pacific dries the lower stratosphere. *Climate Dynamics*, *50*(7), 2813–2827. https://doi.org/10.1007/s00382-017-3774-y

Dobson, G. M. B. (1956). Origin and Distribution of the Polyatomic Molecules in the Atmosphere. *Proceedings of the Royal Society of London Series A*, *236*, 187–193. https://doi.org/10.1098/rspa.1956.0127

Dubé, K., Tegtmeier, S., Ploeger, F., & Walker, K. A. (2025). Hemispheric asymmetry in recent stratospheric age of air changes. *Atmospheric Chemistry and Physics*, *25*(2), 1433–1447. https://doi.org/10.5194/acp-25-1433-2025

de F. Forster, P. M., & Shine, K. P. (1997). Radiative forcing and temperature trends from stratospheric ozone changes. *Journal of Geophysical Research: Atmospheres*, *102*(D9), 10841–10855. https://doi.org/10.1029/96JD03510

Fogt, R. L., & Marshall, G. J. (2020). The Southern Annular Mode: Variability, trends, and climate impacts across the Southern Hemisphere. *WIREs Climate Change*, *11*(4), e652. https://doi.org/10.1002/wcc.652

Forster, P. M. F., Freckleton, R. S., & Shine, K. P. (1997). On aspects of the concept of radiative forcing. *Climate Dynamics*, *13*(7), 547–560. https://doi.org/10.1007/s003820050182

Fu, Q., Lin, P., Solomon, S., & Hartmann, D. L. (2015). Observational evidence of strengthening of the Brewer-Dobson circulation since 1980. *Journal of Geophysical Research: Atmospheres*, *120*(19), 10,214-10,228. https://doi.org/10.1002/2015JD023657

Fu, Qiang. (2013). Bottom up in the tropics. *Nature Climate Change*, *3*(11), 957–958. https://doi.org/10.1038/nclimate2039

Fu, Qiang, & Johanson, C. M. (2005). Satellite-derived vertical dependence of tropical tropospheric temperature trends. *Geophysical Research Letters*, *32*(10). https://doi.org/10.1029/2004GL022266

Fu, Qiang, & Liou, K. N. (1992). On the Correlated k-Distribution Method for Radiative Transfer in Nonhomogeneous Atmospheres. Retrieved from https://journals.ametsoc.org/view/journals/atsc/49/22/1520-0469_1992_049_2139_otcdmf_2_0_co_2.xml

Fu, Qiang, Johanson, C. M., Warren, S. G., & Seidel, D. J. (2004). Contribution of stratospheric cooling to satellite-inferred tropospheric temperature trends. *Nature*, *429*(6987), 55–58. https://doi.org/10.1038/nature02524

Fu, Qiang, Solomon, S., Pahlavan, H. A., & Lin, P. (2019). Observed changes in Brewer–Dobson circulation for 1980–2018. *Environmental Research Letters*, *14*(11), 114026. https://doi.org/10.1088/1748-9326/ab4de7

Fu, Q., S. Solomon, and P. Lin, 2010: On the seasonal dependence of tropical lower-stratospheric temperature trends. Atmos. Chem. Phys., 10, 2643-2653.

Gao, P., Xu, X., & Zhang, X. (2015). Characteristics of the Trends in the Global Tropopause Estimated From COSMIC Radio Occultation Data. *IEEE Transactions on Geoscience and Remote Sensing*, *53*(12), 6813–6822. https://doi.org/10.1109/TGRS.2015.2449338

Garcia, R. R., & Solomon, S. (1983). A numerical model of the zonally averaged dynamical and chemical structure of the middle atmosphere. *Journal of Geophysical Research: Oceans*, *88*(C2), 1379–1400. https://doi.org/10.1029/JC088iC02p01379

Garfinkel, C. I., Aquila, V., Waugh, D. W., & Oman, L. D. (2017). Time-varying changes in the simulated structure of the Brewer–Dobson Circulation. *Atmospheric Chemistry and Physics*, *17*(2), 1313–1327. https://doi.org/10.5194/acp-17-1313-2017

Garny, H., Dameris, M., Randel, W., Bodeker, G. E., & Deckert, R. (2011). Dynamically Forced Increase of Tropical Upwelling in the Lower Stratosphere. *Journal of the Atmospheric Sciences*, *68*(6), 1214–1233. https://doi.org/10.1175/2011JAS3701.1

Gleisner, H., Ringer, M. A., & Healy, S. B. (2022). Monitoring global climate change using GNSS radio occultation. *Npj Climate and Atmospheric Science*, *5*(1), 1–4. https://doi.org/10.1038/s41612-022-00229-7

Hardiman, S. C., Butchart, N., Haynes, P. H., & Hare, S. H. E. (2007). A note on forced versus internal variability of the stratosphere. *Geophysical Research Letters*, *34*(12). https://doi.org/10.1029/2007GL029726

Haynes, P., Hitchcock, P., Hitchman, M., Yoden, S., Hendon, H., Kiladis, G., et al. (2021). The Influence of the Stratosphere on the Tropical Troposphere. *Journal of the Meteorological Society of Japan. Ser. II*, *99*(4), 803–845. https://doi.org/10.2151/jmsj.2021-040

Hersbach, H., Bell, B., Berrisford, P., Hirahara, S., Horányi, A., Muñoz-Sabater, J., et al. (2020). The ERA5 global reanalysis. *Quarterly Journal of the Royal Meteorological Society*, *146*(730), 1999–2049. https://doi.org/10.1002/qj.3803

Hu, Y., Tian, W., Zhang, J., Wang, T., & Xu, M. (2022). Weakening of Antarctic stratospheric planetary wave activities in early austral spring since the early 2000s: a response to sea surface temperature trends. *Atmospheric Chemistry and Physics*, *22*(2), 1575–1600. https://doi.org/10.5194/acp-22-1575-2022

Hu, Y., Xia, Y., & Fu, Q. (2011). Tropospheric temperature response to stratospheric ozone recovery in the 21st century. *Atmospheric Chemistry and Physics*, *11*(15), 7687–7699. https://doi.org/10.5194/acp-11-7687-2011

Iglesias-Suarez, F., Wild, O., Kinnison, D. E., Garcia, R. R., Marsh, D. R., Lamarque, J.-F., et al. (2021). Tropical Stratospheric Circulation and Ozone Coupled to Pacific Multi-Decadal Variability. *Geophysical Research Letters*, *48*(11), e2020GL092162. https://doi.org/10.1029/2020GL092162

Intergovernmental Panel on Climate Change (IPCC) (Ed.). (2023). Changing State of the Climate System. In *Climate Change 2021 – The Physical Science Basis: Working Group I Contribution to the Sixth Assessment Report of the Intergovernmental Panel on Climate Change* (pp. 287–422). Cambridge: Cambridge University Press. https://doi.org/10.1017/9781009157896.004

Ivanciu, I., Matthes, K., Biastoch, A., Wahl, S., & Harlaß, J. (2022). Twenty-first-century Southern Hemisphere impacts of ozone recovery and climate change from the stratosphere to the ocean. *Weather and Climate Dynamics*, *3*(1), 139–171. https://doi.org/10.5194/wcd-3-139-2022

Karoly, D., Cohen, J., Meehl, G., Mitchell, J., Oort, A., Stouffer, R., & Wetherald, R. (1994). An example of fingerprint detection of greenhouse climate change. *Climate Dynamics*, *10*(1), 97–105. https://doi.org/10.1007/BF00210339

Keeling, C. D., Bacastow, R. B., Bainbridge, A. E., Ekdahl Jr., C. A., Guenther, P. R., Waterman, L. S., & Chin, J. F. S. (1976). Atmospheric carbon dioxide variations at Mauna Loa Observatory, Hawaii. *Tellus*, *28*(6), 538–551. https://doi.org/10.1111/j.2153-3490.1976.tb00701.x

Kessenich, H. E., Seppälä, A., & Rodger, C. J. (2023). Potential drivers of the recent large Antarctic ozone holes. *Nature Communications*, *14*(1), 7259. https://doi.org/10.1038/s41467-023-42637-0

Khaykin, S. M., Funatsu, B. M., Hauchecorne, A., Godin-Beekmann, S., Claud, C., Keckhut, P., et al. (2017). Postmillennium changes in stratospheric temperature consistently resolved by GPS radio occultation and AMSU observations. *Geophysical Research Letters*, *44*(14), 7510–7518. https://doi.org/10.1002/2017GL074353

Krzyścin, J., & Czerwińska, A. (2024). Signs of Slowing Recovery of Antarctic Ozone Hole in Recent Late Winter–Early Spring Seasons (2020–2023). *Atmosphere*, *15*(1), 80. https://doi.org/10.3390/atmos15010080

Kuo, Y.-H., Wee, T.-K., Sokolovskiy, S., Rocken, C., Schreiner, W., Hunt, D., & Anthes, R. A. (2004). Inversion and Error Estimation of GPS Radio Occultation Data. *Journal of the Meteorological Society of Japan. Ser. II*, *82*(1B), 507–531. https://doi.org/10.2151/jmsj.2004.507

Kursinski, E. R., Hajj, G. A., Schofield, J. T., Linfield, R. P., & Hardy, K. R. (1997). Observing Earth's atmosphere with radio occultation measurements using the Global Positioning System. *Journal of Geophysical Research: Atmospheres*, *102*(D19), 23429–23465. https://doi.org/10.1029/97JD01569

Kuttippurath, J., & Nair, P. J. (2017). The signs of Antarctic ozone hole recovery. *Scientific Reports*, *7*(1), 585. https://doi.org/10.1038/s41598-017-00722-7

Ladstädter, F., Steiner, A. K., & Gleisner, H. (2023). Resolving the 21st century temperature trends of the upper troposphere–lower stratosphere with satellite observations. *Scientific Reports*, *13*(1), 1306. https://doi.org/10.1038/s41598-023-28222-x

Lan, X., K.W. Thoning, and E.J. Dlugokencky: Trends in globally-averaged CH4, N2O, and SF6 determined from NOAA Global Monitoring Laboratory measurements. Version 2024-08, https://doi.org/10.15138/P8XG-AA10

Lawrence, Z. D., Abalos, M., Ayarzagüena, B., Barriopedro, D., Butler, A. H., Calvo, N., et al. (2022). Quantifying stratospheric biases and identifying their potential sources in subseasonal forecast systems. *Weather and Climate Dynamics*, *3*(3), 977–1001. https://doi.org/10.5194/wcd-3-977-2022

Leroy, S. S., Ao, C. O., & Verkhoglyadova, O. P. (2018). Temperature Trends and Anomalies in Modern Satellite Data: Infrared Sounding and GPS Radio Occultation. *Journal of Geophysical Research: Atmospheres*, *123*(20), 11,431-11,444. https://doi.org/10.1029/2018JD028990

Lim, E.-P., Hendon, H. H., Butler, A. H., Thompson, D. W. J., Lawrence, Z. D., Scaife, A. A., et al. (2021). The 2019 Southern Hemisphere Stratospheric Polar Vortex Weakening and Its Impacts. https://doi.org/10.1175/BAMS-D-20-0112.1

Lin, J., & Emanuel, K. (2024). Why the lower stratosphere cools when the troposphere warms. *Proceedings of the National Academy of Sciences*, *121*(11), e2319228121. https://doi.org/10.1073/pnas.2319228121

Livesey, N. J., Read, W. G., Froidevaux, L., Lambert, A., Santee, M. L., Schwartz, M. J., et al. (2021). Investigation and amelioration of long-term instrumental drifts in water vapor and nitrous oxide measurements from the Aura Microwave Limb Sounder (MLS) and their implications for studies of variability and trends. *Atmospheric Chemistry and Physics*, *21*(20), 15409–15430. https://doi.org/10.5194/acp-21-15409-2021

Maycock, A. C. (2016). The contribution of ozone to future stratospheric temperature trends. *Geophysical Research Letters*, *43*(9), 4609–4616. https://doi.org/10.1002/2016GL068511

Maycock, A. C., Randel, W. J., Steiner, A. K., Karpechko, A. Y., Christy, J., Saunders, R., et al. (2018). Revisiting the Mystery of Recent Stratospheric Temperature Trends. *Geophysical Research Letters*, *45*(18), 9919–9933. https://doi.org/10.1029/2018GL078035

Mahieu, E., Chipperfield, M. P., Notholt, J., Reddmann, T., Anderson, J., Bernath, P. F., et al. (2014). Recent Northern Hemisphere stratospheric HCl increase due to atmospheric circulation changes. *Nature*, *515*(7525), 104–107. https://doi.org/10.1038/nature13857

Manabe, S., & Wetherald, R. T. (1967). Thermal Equilibrium of the Atmosphere with a Given Distribution of Relative Humidity. Retrieved from

https://journals.ametsoc.org/view/journals/atsc/24/3/1520-0469_1967_024_0241_teotaw_2_0_co_2.xml

McLandress, C., Jonsson, A. I., Plummer, D. A., Reader, M. C., Scinocca, J. F., & Shepherd, T. G. (2010). Separating the Dynamical Effects of Climate Change and Ozone Depletion. Part I: Southern Hemisphere Stratosphere. *Journal of Climate*, *23*(18), 5002–5020. https://doi.org/10.1175/2010JCLI3586.1

McLandress, C., Shepherd, T. G., Scinocca, J. F., Plummer, D. A., Sigmond, M., Jonsson, A. I., & Reader, M. C. (2011). Separating the Dynamical Effects of Climate Change and Ozone Depletion. Part II: Southern Hemisphere Troposphere. *Journal of Climate*, *24*(6), 1850–1868. https://doi.org/10.1175/2010JCLI3958.1

Meinshausen, M., Smith, S. J., Calvin, K., Daniel, J. S., Kainuma, M. L. T., Lamarque, J.-F., et al. (2011). The RCP greenhouse gas concentrations and their extensions from 1765 to 2300. *Climatic Change*, *109*(1), 213. https://doi.org/10.1007/s10584-011-0156-z

Ming, A., & Hitchcock, P. (2022). What Contributes to the Inter-Annual Variability in Tropical Lower Stratospheric Temperatures? *Journal of Geophysical Research: Atmospheres*, *127*(1), e2021JD035548. https://doi.org/10.1029/2021JD035548

Mitchell, D. M., Lo, Y. T. E., Seviour, W. J. M., Haimberger, L., & Polvani, L. M. (2020). The vertical profile of recent tropical temperature trends: Persistent model biases in the context of internal variability. *Environmental Research Letters*, *15*(10), 1040b4. https://doi.org/10.1088/1748-9326/ab9af7

Montzka, S. A., Dutton, G. S., Yu, P., Ray, E., Portmann, R. W., Daniel, J. S., et al. (2018). An unexpected and persistent increase in global emissions of ozone-depleting CFC-11. *Nature*, *557*(7705), 413–417. https://doi.org/10.1038/s41586-018-0106-2

Newman, P. A., & Nash, E. R. (2005). The Unusual Southern Hemisphere Stratosphere Winter of 2002. https://doi.org/10.1175/JAS-3323.1

Newman, P. A., Nash, E. R., Kawa, S. R., Montzka, S. A., & Schauffler, S. M. (2006). When will the Antarctic ozone hole recover? *Geophysical Research Letters*, *33*(12). https://doi.org/10.1029/2005GL025232

Olsen, M. A., Schoeberl, M. R., & Nielsen, J. E. (2007). Response of stratospheric circulation and stratosphere-troposphere exchange to changing sea surface temperatures. *Journal of Geophysical Research: Atmospheres*, *112*(D16). https://doi.org/10.1029/2006JD008012

Orbe, C., Wargan, K., Pawson, S., & Oman, L. D. (2020). Mechanisms Linked to Recent Ozone Decreases in the Northern Hemisphere Lower Stratosphere. *Journal of Geophysical Research: Atmospheres*, *125*(9), e2019JD031631. https://doi.org/10.1029/2019JD031631

Perliski, L. M., Solomon, S., & London, J. (1989). On the interpretation of seasonal variations of stratospheric ozone. *Planetary and Space Science*, *37*(12), 1527–1538. https://doi.org/10.1016/0032-0633(89)90143-8

Ploeger, F., & Garny, H. (2022). Hemispheric asymmetries in recent changes in the stratospheric circulation. *Atmospheric Chemistry and Physics*, *22*(8), 5559–5576. https://doi.org/10.5194/acp-22-5559-2022

Polvani, L. M., Wang, L., Abalos, M., Butchart, N., Chipperfield, M. P., Dameris, M., et al. (2019). Large Impacts, Past and Future, of Ozone-Depleting Substances on Brewer-Dobson Circulation Trends: A Multimodel Assessment. *Journal of Geophysical Research: Atmospheres*, *124*(13), 6669–6680. https://doi.org/10.1029/2018JD029516

Polvani, Lorenzo M., Abalos, M., Garcia, R., Kinnison, D., & Randel, W. J. (2018). Significant Weakening of Brewer-Dobson Circulation Trends Over the 21st Century as a Consequence

of the Montreal Protocol. *Geophysical Research Letters*, *45*(1), 401–409. https://doi.org/10.1002/2017GL075345

Randel, W. J., & Wu, F. (2015). Variability of Zonal Mean Tropical Temperatures Derived from a Decade of GPS Radio Occultation Data. *Journal of the Atmospheric Sciences*, *72*(3), 1261–1275. https://doi.org/10.1175/JAS-D-14-0216.1

Randel, W. J., Garcia, R. R., Calvo, N., & Marsh, D. (2009). ENSO influence on zonal mean temperature and ozone in the tropical lower stratosphere. *Geophysical Research Letters*, *36*(15). https://doi.org/10.1029/2009GL039343

Randel, W. J., Polvani, L., Wu, F., Kinnison, D. E., Zou, C.-Z., & Mears, C. (2017). Troposphere-Stratosphere Temperature Trends Derived From Satellite Data Compared With Ensemble Simulations From WACCM. *Journal of Geophysical Research: Atmospheres*, *122*(18), 9651–9667. https://doi.org/10.1002/2017JD027158

Read, W. G., Lambert, A., Bacmeister, J., Cofield, R. E., Christensen, L. E., Cuddy, D. T., et al. (2007). Aura Microwave Limb Sounder upper tropospheric and lower stratospheric H2O and relative humidity with respect to ice validation. *Journal of Geophysical Research (Atmospheres)*, *112*, D24S35. https://doi.org/10.1029/2007JD008752

Rigby, M., Park, S., Saito, T., Western, L. M., Redington, A. L., Fang, X., et al. (2019). Increase in CFC-11 emissions from eastern China based on atmospheric observations. *Nature*, *569*(7757), 546–550. https://doi.org/10.1038/s41586-019-1193-4

Robertson, F., Revell, L. E., Douglas, H., Archibald, A. T., Morgenstern, O., & Frame, D. (2023). Signal-To-Noise Calculations of Emergence and De-Emergence of Stratospheric Ozone Depletion. *Geophysical Research Letters*, *50*(16), e2023GL104246. https://doi.org/10.1029/2023GL104246

Santer, B. D., Wigley, T. M. L., Mears, C., Wentz, F. J., Klein, S. A., Seidel, D. J., et al. (2005). Amplification of Surface Temperature Trends and Variability in the Tropical Atmosphere. *Science*, *309*(5740), 1551–1556. https://doi.org/10.1126/science.1114867

Santer, Benjamin D., Po-Chedley, S., Zhao, L., Zou, C.-Z., Fu, Q., Solomon, S., et al. (2023). Exceptional stratospheric contribution to human fingerprints on atmospheric temperature. *Proceedings of the National Academy of Sciences*, *120*(20), e2300758120. https://doi.org/10.1073/pnas.2300758120

Scherllin-Pirscher, B., Steiner, A. K., Anthes, R. A., Alexander, M. J., Alexander, S. P., Biondi, R., et al. (2021). Tropical Temperature Variability in the UTLS: New Insights from GPS Radio Occultation Observations. *Journal of Climate*, *34*(8), 2813–2838. https://doi.org/10.1175/JCLI-D-20-0385.1

Seidel, D. J., Gillett, N. P., Lanzante, J. R., Shine, K. P., & Thorne, P. W. (2011). Stratospheric temperature trends: our evolving understanding. *WIREs Climate Change*, *2*(4), 592–616. https://doi.org/10.1002/wcc.125

Shangguan, M., Wang, W., & Jin, S. (2019). Variability of temperature and ozone in the upper troposphere and lower stratosphere from multi-satellite observations and reanalysis data. *Atmospheric Chemistry and Physics*, *19*(10), 6659–6679. https://doi.org/10.5194/acp-19-6659-2019

Shepherd, T. G. (2007). Transport in the Middle Atmosphere. *Journal of the Meteorological Society of Japan. Ser. II*, *85B*, 165–191. https://doi.org/10.2151/jmsj.85B.165

Solomon, S., Garcia, R.R., Rowland, F.S. and Wuebbles, D.J., 1986. On the depletion of Antarctic ozone. *Nature*, *321*(6072), pp.755-758.

Solomon, S. (1999). Stratospheric ozone depletion: A review of concepts and history. *Reviews of Geophysics*, *37*(3), 275–316. https://doi.org/10.1029/1999RG900008

Solomon, S., Ivy, D. J., Kinnison, D., Mills, M. J., Neely, R. R., & Schmidt, A. (2016). Emergence of healing in the Antarctic ozone layer. *Science*, *353*(6296), 269–274. https://doi.org/10.1126/science.aae0061

Solomon, S., Ivy, D., Gupta, M., Bandoro, J., Santer, B., Fu, Q., et al. (2017). Mirrored changes in Antarctic ozone and stratospheric temperature in the late 20th versus early 21st centuries. *Journal of Geophysical Research: Atmospheres*, *122*(16), 8940–8950. https://doi.org/10.1002/2017JD026719

Solomon, S., Dube, K., Stone, K., Yu, P., Kinnison, D., Toon, O. B., et al. (2022). On the stratospheric chemistry of midlatitude wildfire smoke. *Proceedings of the National Academy of Sciences*, *119*(10), e2117325119. https://doi.org/10.1073/pnas.2117325119

Solomon, S., Stone, K., Yu, P., Murphy, D. M., Kinnison, D., Ravishankara, A. R., & Wang, P. (2023). Chlorine activation and enhanced ozone depletion induced by wildfire aerosol. *Nature*, *615*(7951), 259–264. https://doi.org/10.1038/s41586-022-05683-0

SPARC, 2022: SPARC Reanalysis Intercomparison Project (S-RIP) Final Report. Masatomo Fujiwara, Gloria L. Manney, Lesley J. Gray, and Jonathon S. Wright (Eds.), SPARC Report No. 10, WCRP-6/2021, doi: 10.17874/800dee57d13, available at www.sparc-climate.org/publications/sparc-reports.

Steiner, A. K., Hunt, D., Ho, S.-P., Kirchengast, G., Mannucci, A. J., Scherllin-Pirscher, B., et al. (2013). Quantification of structural uncertainty in climate data records from GPS radio occultation. *Atmospheric Chemistry and Physics*, *13*(3), 1469–1484. https://doi.org/10.5194/acp-13-1469-2013

Steiner, A. K., Ladstädter, F., Randel, W. J., Maycock, A. C., Fu, Q., Claud, C., et al. (2020). Observed Temperature Changes in the Troposphere and Stratosphere from 1979 to 2018. *Journal of Climate*, *33*(19), 8165–8194. https://doi.org/10.1175/JCLI-D-19-0998.1

Steiner, Andrea K., Ladstädter, F., Ao, C. O., Gleisner, H., Ho, S.-P., Hunt, D., et al. (2020). Consistency and structural uncertainty of multi-mission GPS radio occultation records. *Atmospheric Measurement Techniques*, *13*(5), 2547–2575. https://doi.org/10.5194/amt-13-2547-2020

Stiller, G. P., von Clarmann, T., Haenel, F., Funke, B., Glatthor, N., Grabowski, U., et al. (2012). Observed temporal evolution of global mean age of stratospheric air for the 2002 to 2010 period. *Atmospheric Chemistry and Physics*, *12*(7), 3311–3331. https://doi.org/10.5194/acp-12-3311-2012

Stiller, Gabriele P., Fierli, F., Ploeger, F., Cagnazzo, C., Funke, B., Haenel, F. J., et al. (2017). Shift of subtropical transport barriers explains observed hemispheric asymmetry of decadal trends of age of air. *Atmospheric Chemistry and Physics*, *17*(18), 11177–11192. https://doi.org/10.5194/acp-17-11177-2017

Stocker, M., Ladstädter, F., & Steiner, A. K. (2021). Observing the climate impact of large wildfires on stratospheric temperature. *Scientific Reports*, *11*(1), 22994. https://doi.org/10.1038/s41598-021-02335-7

Stocker, M., Steiner, A. K., Ladstädter, F., Foelsche, U., & Randel, W. J. (2024). Strong persistent cooling of the stratosphere after the Hunga eruption. *Communications Earth & Environment*, *5*(1), 1–11. https://doi.org/10.1038/s43247-024-01620-3

Stone, K. A., Solomon, S., Kinnison, D. E., & Mills, M. J. (2021). On Recent Large Antarctic Ozone Holes and Ozone Recovery Metrics. *Geophysical Research Letters*, *48*(22), e2021GL095232. https://doi.org/10.1029/2021GL095232

Sweeney, A., & Fu, Q. (2024). Interannual Variability of Zonal Mean Temperature, Water Vapor, and Clouds in the Tropical Tropopause Layer. *Journal of Geophysical Research: Atmospheres*, *129*(3), e2023JD039002. https://doi.org/10.1029/2023JD039002

Szeląg, M. E., Sofieva, V. F., Degenstein, D., Roth, C., Davis, S., & Froidevaux, L. (2020). Seasonal stratospheric ozone trends over 2000–2018 derived from several merged data sets. *Atmospheric Chemistry and Physics*, *20*(11), 7035–7047. https://doi.org/10.5194/acp-20-7035-2020

Tao, M., Konopka, P., Wright, J. S., Liu, Y., Bian, J., Davis, S. M., et al. (2023). Multi-decadal variability controls short-term stratospheric water vapor trends. *Communications Earth & Environment*, *4*(1), 1–10. https://doi.org/10.1038/s43247-023-01094-9

Thompson, D. W. J., Seidel, D. J., Randel, W. J., Zou, C.-Z., Butler, A. H., Mears, C., et al. (2012). The mystery of recent stratospheric temperature trends. *Nature*, *491*(7426), 692–697. https://doi.org/10.1038/nature11579

Thompson, D. W. J., & Wallace, J. M. (2000). Annular Modes in the Extratropical Circulation. Part I: Month-to-Month Variability. Retrieved from https://journals.ametsoc.org/view/journals/clim/13/5/1520-0442_2000_013_1000_amitec_2.0.co_2.xml

Tseng, H.-H., & Fu, Q. (2017). Temperature Control of the Variability of Tropical Tropopause Layer Cirrus Clouds. *Journal of Geophysical Research: Atmospheres*, *122*(20), 11,062-11,075. https://doi.org/10.1002/2017JD027093

Ueyama, R., Gerber, E. P., Wallace, J. M., & Frierson, D. M. W. (2013). The Role of High-Latitude Waves in the Intraseasonal to Seasonal Variability of Tropical Upwelling in the Brewer–Dobson Circulation. *Journal of the Atmospheric Sciences*, *70*(6), 1631–1648. https://doi.org/10.1175/JAS-D-12-0174.1

Vallis, G. K., Zurita-Gotor, P., Cairns, C., & Kidston, J. (2015). Response of the large-scale structure of the atmosphere to global warming. *Quarterly Journal of the Royal Meteorological Society*, *141*(690), 1479–1501. https://doi.org/10.1002/qj.2456

Vergados, P., Ao, C. O., Mannucci, A. J., & Kursinski, E. R. (2021). Quantifying the Tropical Upper Tropospheric Warming Amplification Using Radio Occultation Measurements. *Earth and Space Science*, *8*(2), e2020EA001597. https://doi.org/10.1029/2020EA001597

Villamayor, J., Iglesias-Suarez, F., Cuevas, C. A., Fernandez, R. P., Li, Q., Abalos, M., et al. (2023). Very short-lived halogens amplify ozone depletion trends in the tropical lower stratosphere. *Nature Climate Change*, *13*(6), 554–560. https://doi.org/10.1038/s41558-023-01671-y

Wallace, J. M., Panetta, R. L., & Estberg, J. (1993). Representation of the Equatorial Stratospheric Quasi-Biennial Oscillation in EOF Phase Space. *Journal of the Atmospheric Sciences*, *50*(12), 1751–1762. https://doi.org/10.1175/1520-0469(1993)050<1751:ROTESQ>2.0.CO;2

Wang, P., Solomon, S., & Stone, K. (2023). Stratospheric chlorine processing after the 2020 Australian wildfires derived from satellite data. *Proceedings of the National Academy of Sciences*, *120*(11), e2213910120. https://doi.org/10.1073/pnas.2213910120

Wang, P., Solomon, S., Santer, B., Kinnison, D., Fu, Q., Stone, K., et al. (2025, August 20). Fingerprinting the Robust Recovery of Antarctic Ozone. Nature (in press). https://doi.org/10.21203/rs.3.rs-4876981/v1

Wang, W., Matthes, K., Omrani, N.-E., & Latif, M. (2016). Decadal variability of tropical tropopause temperature and its relationship to the Pacific Decadal Oscillation. *Scientific Reports*, *6*(1), 29537. https://doi.org/10.1038/srep29537

Weyland, F., Hoor, P., Kunkel, D., Birner, T., Plöger, F., and Turhal, K.: Long-term changes in the thermodynamic structure of the lowermost stratosphere inferred from reanalysis data, Atmos. Chem. Phys., 25, 1227–1252, https://doi.org/10.5194/acp-25-1227-2025, 2025.

Wolter, K., & Timlin, M. S. (2011). El Niño/Southern Oscillation behaviour since 1871 as diagnosed in an extended multivariate ENSO index (MEI.ext). *International Journal of Climatology*, *31*(7), 1074–1087. https://doi.org/10.1002/joc.2336

World Meteorological Organization (WMO). *Scientific Assessment of Ozone Depletion: 2010* (World Meteorological Organization, 2011).

World Meteorological Organization (WMO), Executive Summary. *Scientific Assessment of Ozone Depletion: 2022*, GAW Report No. 278, 56 pp., WMO, Geneva, Switzerland, 2022.

Xia, Y., Xu, W., Hu, Y., & Xie, F. (2020). Southern-Hemisphere high-latitude stratospheric warming revisit. *Climate Dynamics*, *54*(3), 1671–1682. https://doi.org/10.1007/s00382-019-05083-7

Yook, S., Thompson, D. W. J., & Solomon, S. (2022). Climate Impacts and Potential Drivers of the Unprecedented Antarctic Ozone Holes of 2020 and 2021. *Geophysical Research Letters*, *49*(10), e2022GL098064. https://doi.org/10.1029/2022GL098064

Yulaeva, E., Holton, J. R., & Wallace, J. M. (1994). On the Cause of the Annual Cycle in Tropical Lower-Stratospheric Temperatures. *Journal of the Atmospheric Sciences*, *51*(2), 169–174. https://doi.org/10.1175/1520-0469(1994)051<0169:OTCOTA>2.0.CO;2

Zambri, B., Solomon, S., Thompson, D. W. J., & Fu, Q. (2021). Emergence of Southern Hemisphere stratospheric circulation changes in response to ozone recovery. *Nature Geoscience*, *14*(9), 638–644. https://doi.org/10.1038/s41561-021-00803-3

Zhang, J., Wang, P., Kinnison, D., Solomon, S., Guan, J., Stone, K., & Zhu, Y. (2024). Stratospheric Chlorine Processing After the Unprecedented Hunga Tonga Eruption. *Geophysical Research Letters*, *51*(17), e2024GL108649. https://doi.org/10.1029/2024GL108649

Zolghadrshojaee, M., Tegtmeier, S., Davis, S. M., & Pilch Kedzierski, R. (2024). Variability and long-term changes in tropical cold-point temperature and water vapor. *Atmospheric Chemistry and Physics*, *24*(12), 7405–7419. https://doi.org/10.5194/acp-24-7405-2024

Zuev, V. V., Maslennikova, E. A., Savelieva, E. S., & Pavlinsky, A. V. (2024). Sensitivity of the Antarctic Polar Vortex to Temperature Changes in the Lower Subtropical Stratosphere. *Atmospheric and Oceanic Optics*, *37*(1), 99–102. https://doi.org/10.1134/S1024856023700124

Journal of Geophysical Research: Atmospheres

Supporting Information for

Recent Warming of Southern Hemisphere Subtropical Lower Stratosphere and Antarctic Ozone Healing

Aodhan Sweeney, Qiang Fu, Susan Solomon, Stephen Po-Chedley, Bill Randel, Andrea Steiner, Pu Lin, Thomas Birner, Sean Davis, Peidong Wang

[1]University of Washington, Department of Atmospheric Sciences

Contents of this file

Introduction

This supporting information consists of 17 figures associated with the primary document.

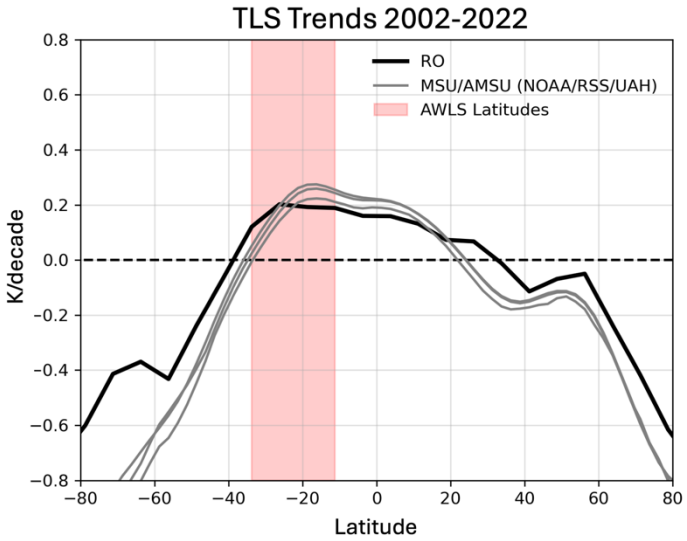

Supplementary Figure 1: Trends of temperature in the lower stratosphere (TLS) based on Microwave Sounding Units (MSU/AMSU) observations from three datasets—NOAA STAR, Remote Sensing Systems (RSS), and University of Alabama Huntsville (UAH) (thin grey lines). The synthetic RO TLS trends (thick black line) are derived by applying the TLS weighting function to the RO measurements. The AWLS latitudes are highlighted by the red rectangle.

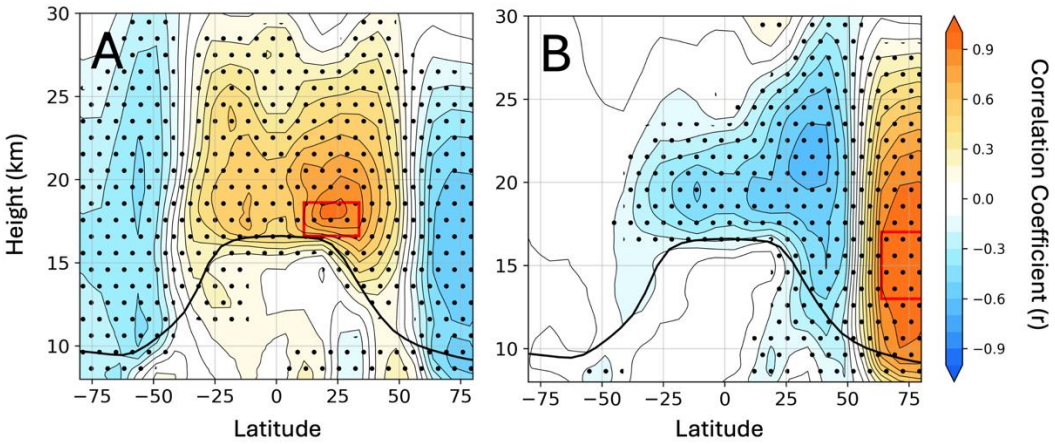

Supplementary Figure 2: Same as Fig. 2 but for the Northern Hemisphere counterparts.

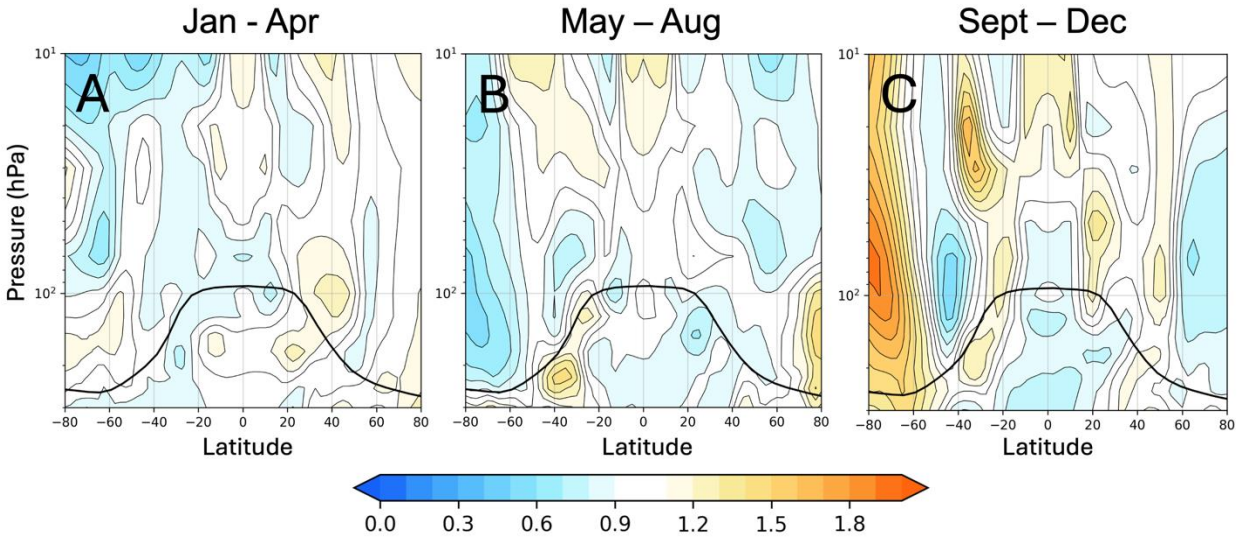

Supplementary Figure 3: Ratio of the standard deviation of detrended monthly temperature anomalies in the ODS period (2002-2022) and that of the pre-ODS period (1955-1975) based on ERA5 data for **(A)** January-April, **(B)** May–August, and **(C)** September–December. Red (blue) colors show the regions where the standard deviation is larger (smaller) during 2002-2022 compared to the 1955-1975.

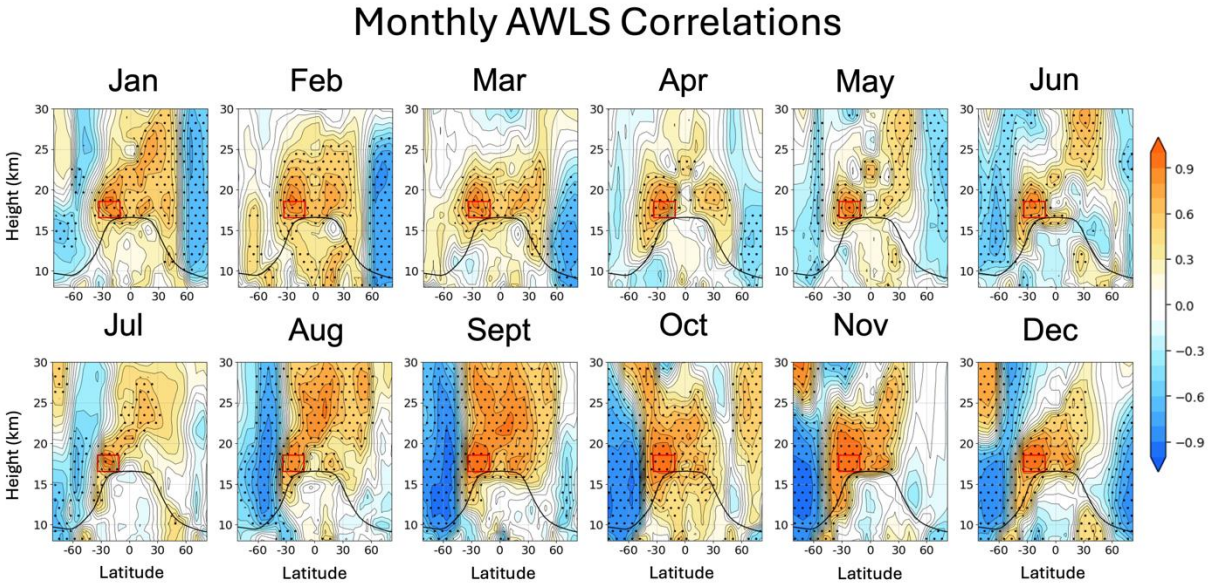

Supplementary Figure 4: Same as Fig. 2A but for monthly correlations with the AWLS time series.

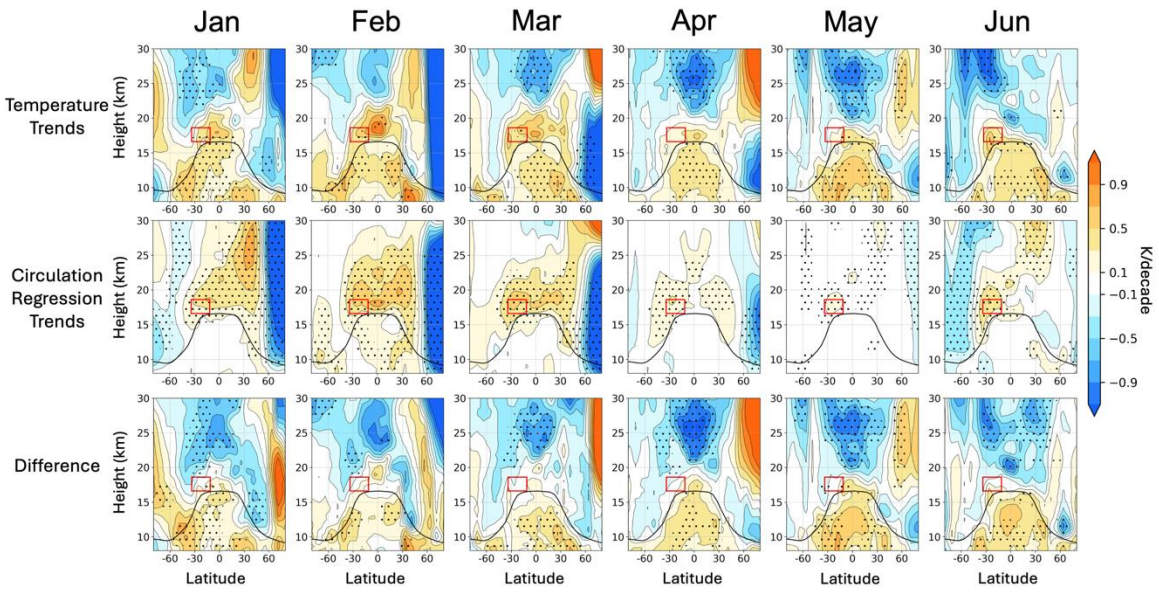

Supplementary Figure 5: Same as Figure 6 but for monthly temperature trends from January-June.

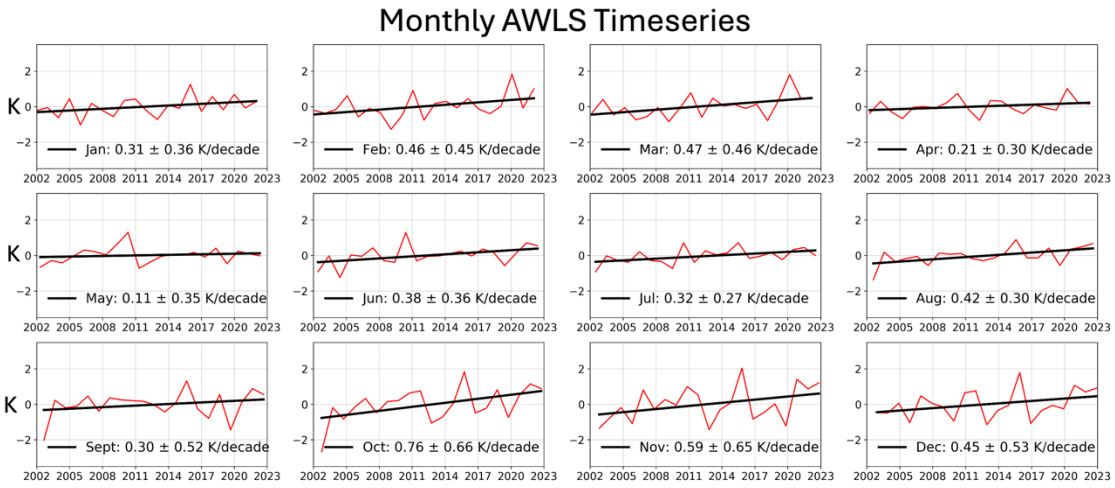

Supplementary Figure 6: AWLS timeseries and trends for each calendar month derived from RO observations.

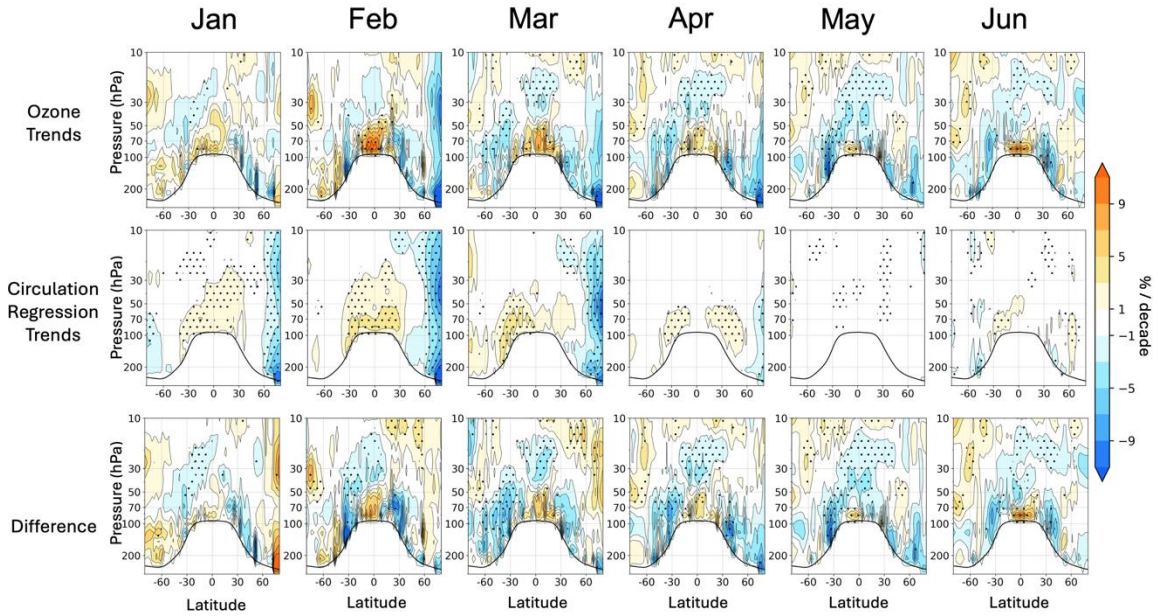

Supplementary Figure 7: Same as Figure 7 but for January-June.

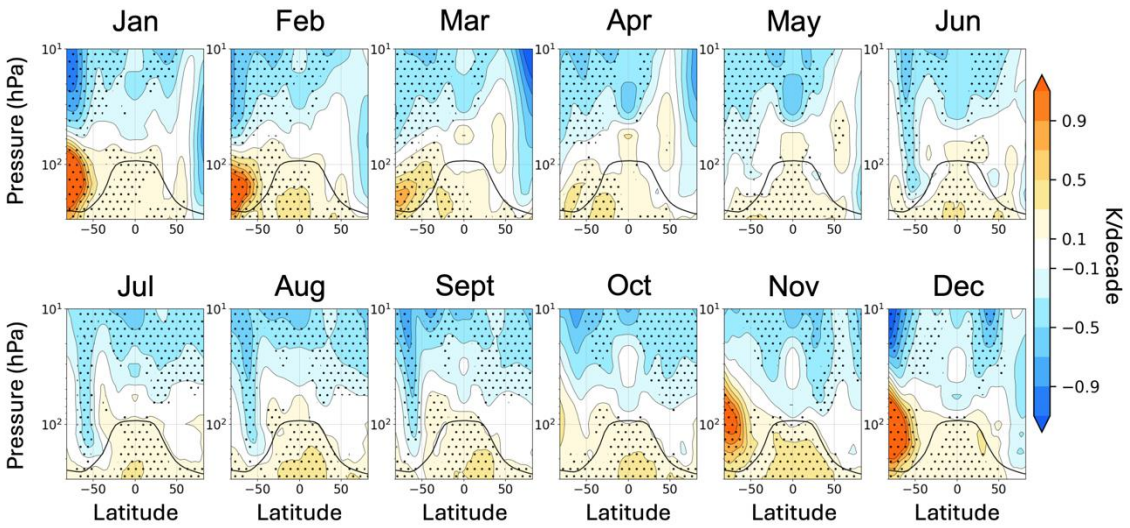

Supplementary Figure 8: Monthly zonal mean temperature trends from the CESM1-WACCM 10-member ensemble mean over 2002-2022.

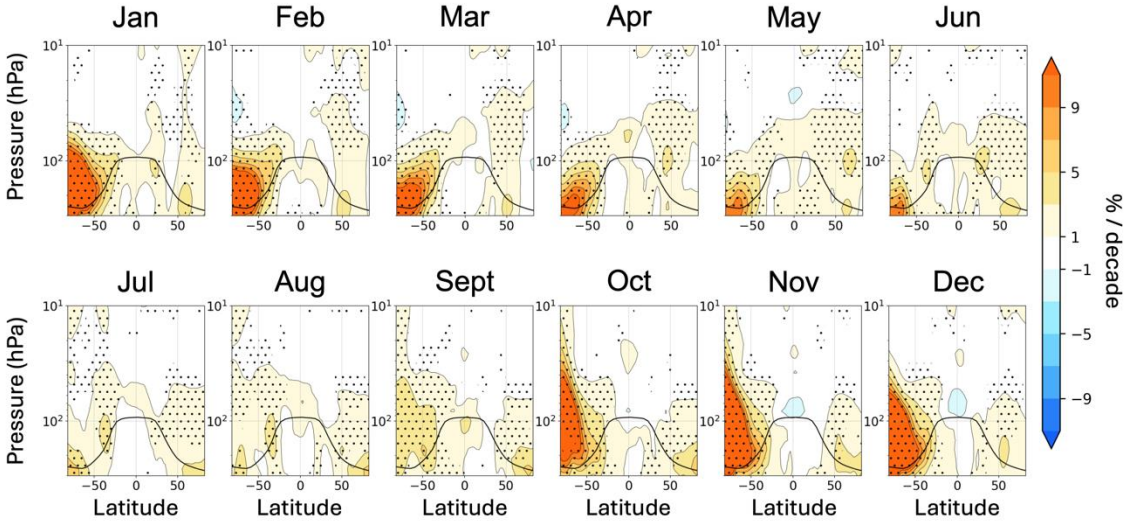

Supplementary Figure 9: Monthly zonal mean ozone trends from the CESM1-WACCM 10-member ensemble mean over 2002-2022.

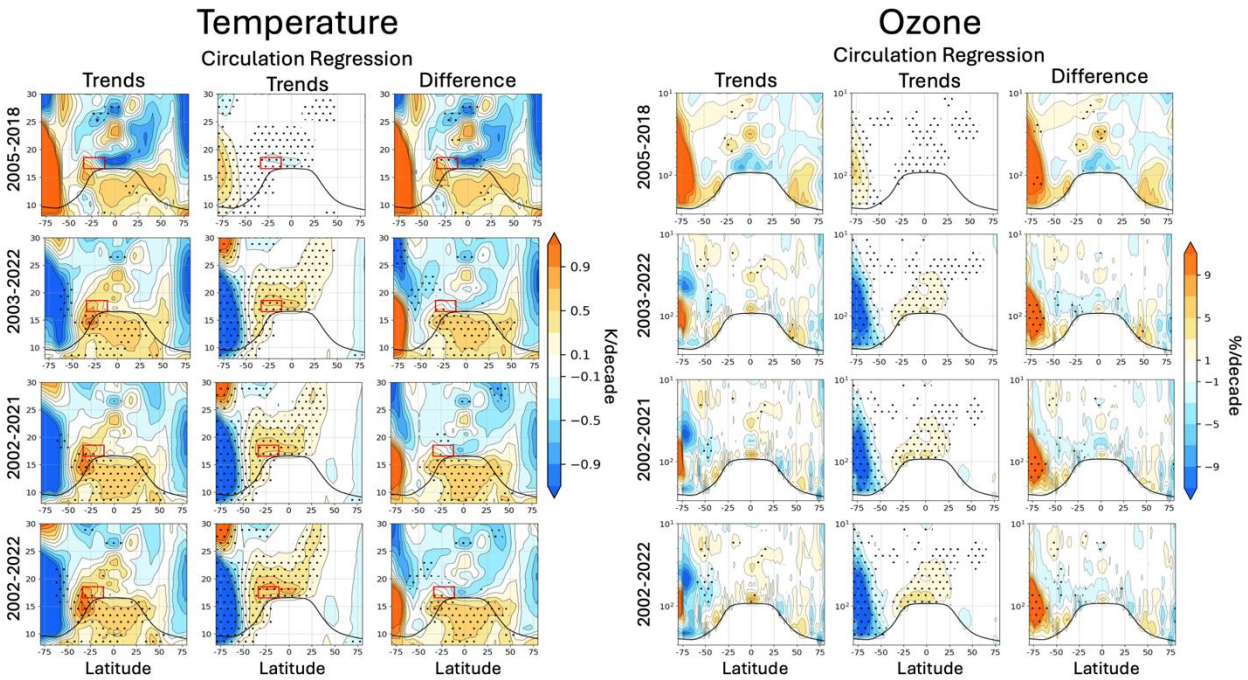

Supplementary Figure 10: Same as Fig. 10 but for November trends.

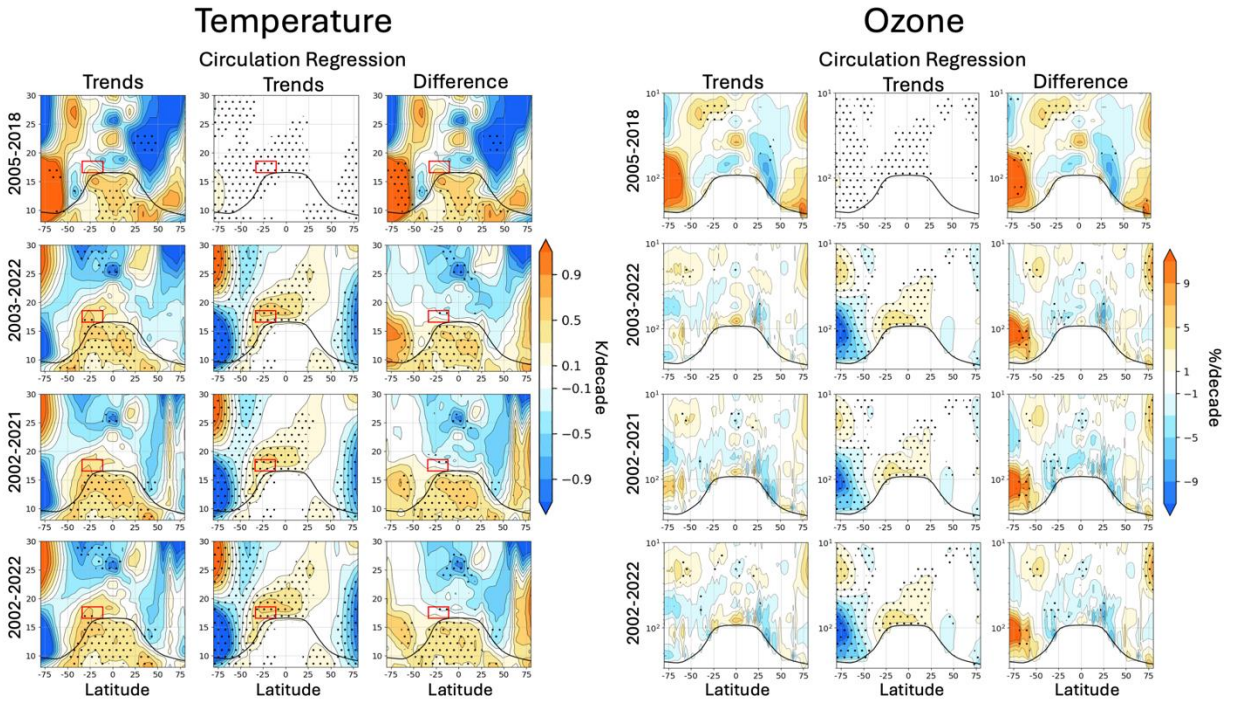

Supplementary Figure 11: Same as Fig. 10 but for December trends.

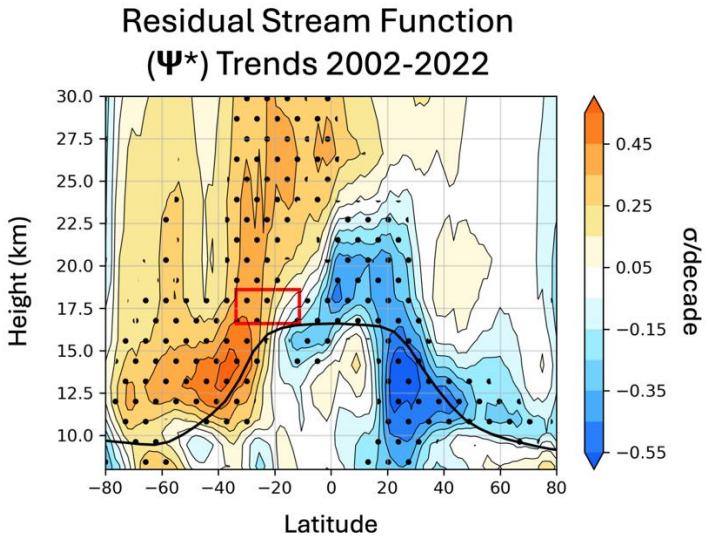

Supplementary Figure 12: Changes from 2002-2022 in the TEM residual stream function from the ERA5 reanalysis. Trends are shown after dividing by the standard deviation of the interannual variability and are thus shown in units of σ/decade. The black line shows the climatological tropopause height.

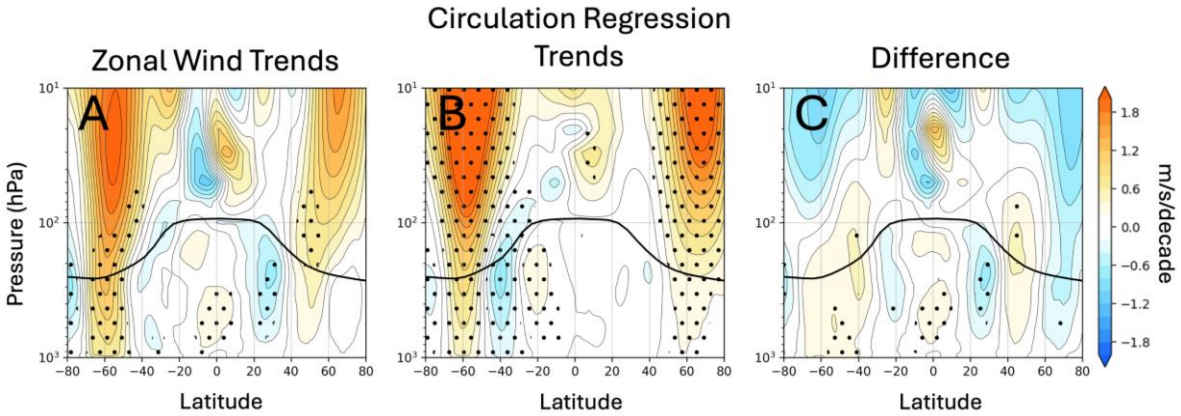

Supplementary Figure 13: (A) ERA5 zonal wind trends. (B) Trends resulting from the circulation regression performed on zonal wind. (C) Difference (i.e., C = A - B).

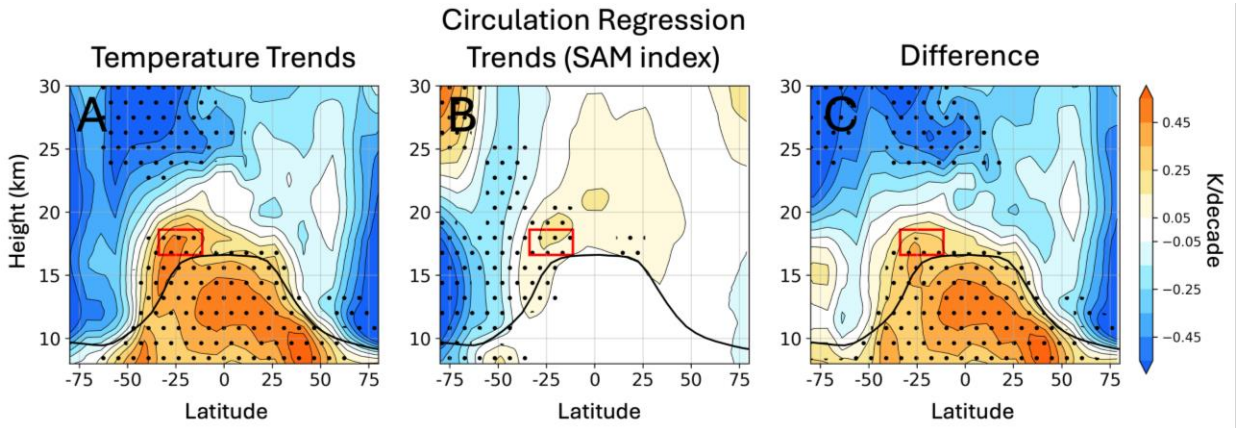

Supplementary Figure 14: Adaption of circulation regression applied to monthly temperature anomalies by replacing AWLS timeseries with the SAM index. (A) Observed temperature trends, (B) those obtained from the adapted circulation regression, (C) difference (i.e., C = A – B).

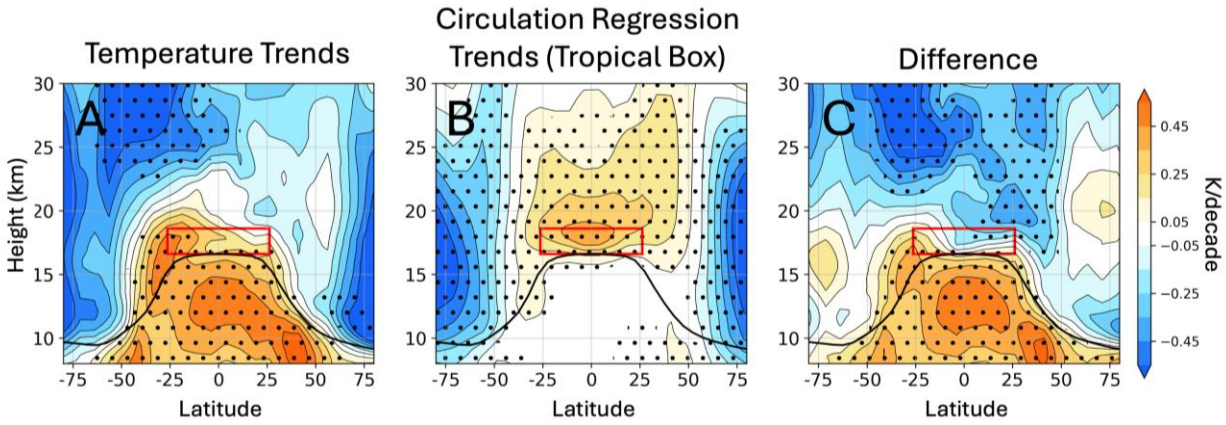

Supplementary Figure 15: Adaption of the circulation regression applied to monthly temperature anomalies in UTLS, replacing the AWLS timeseries with tropical monthly temperature anomalies in the red box.

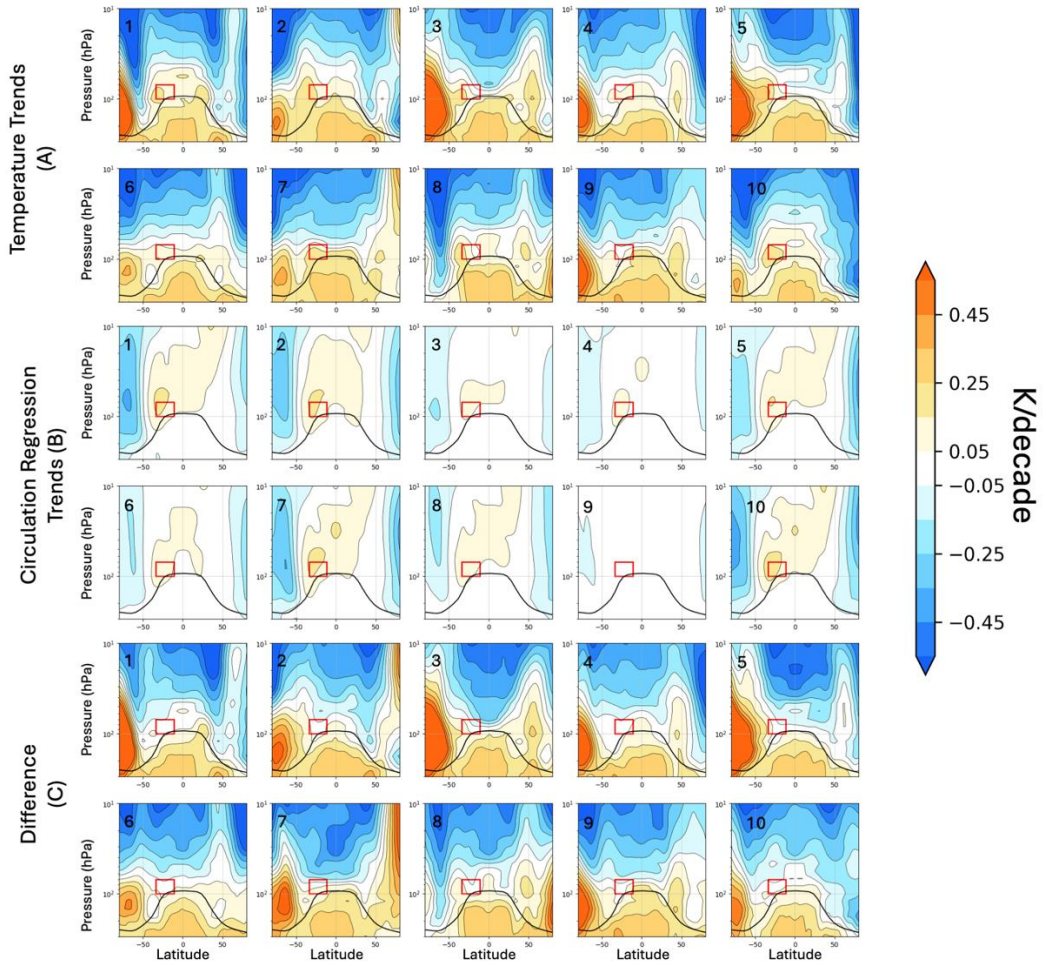

Supplementary Figure 16: Application of the circulation regression to simulated temperature monthly anomalies in each of the 10 members of the CESM1-WACCM ensemble from 2002-2022.

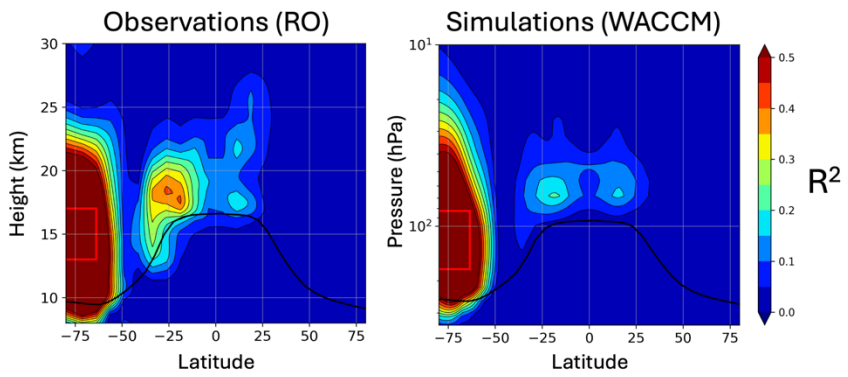

Supplementary Figure 17: Comparison of observed and simulated square of correlation coefficient, R^2, between detrended monthly temperature anomalies in the Antarctic lower stratosphere (red box) and UTLS temperatures. For WACCM, R^2 is first derived for each ensemble member and then averaged. The R^2 from individual members is very similar.